Mother centrioles generate a local pulse of Polo/PLK1 activity to initiate mitotic centrosome assembly

Siu-Shing Wong[1†], Zachary M. Wilmott[1,2†], Saroj Saurya[1], Felix Y. Zhou[3], Kwai-Yin Chau[4], Alain Goriely[2], Jordan W. Raff[1*]

Affiliation:

[1]Sir William Dunn School of Pathology, University of Oxford, Oxford, UK

[2]Mathematical Institute, University of Oxford, Oxford, UK

[3]Ludwig Institute for Cancer Research, Nuffield Department of Clinical Medicine, University of Oxford, Oxford, UK.

[4]Department of Computer Science, University of Bath, Bath, UK

[†] These authors contributed equally to this work

* Correspondence: jordan.raff@path.ox.ac.uk

Key Words: centriole, centrosome, PCM, PLK1, mitosis, cell cycle, oscillator

Abstract

Mitotic centrosomes are formed when centrioles recruit large amounts of pericentriolar material (PCM) around themselves. This centrosome "maturation" requires the centrioles and also Polo/PLK1 protein kinase. The PCM comprises several hundred proteins and, in *Drosophila*, Polo cooperates with the conserved centrosome proteins Spd-2/CEP192 and Cnn/CDK5RAP2 to assemble a PCM scaffold around the mother centriole that then recruits other PCM client proteins. We show here that in *Drosophila* syncytial blastoderm embryos, centrosomal Polo levels rise and fall during the assembly process—peaking, and then starting to decline, even as levels of the PCM scaffold continue to rise. Experiments and mathematical modelling indicate that a centriolar pulse of Polo activity, potentially generated by the interaction between Polo and its centriole receptor Ana1 (CEP295 in humans), could explain these unexpected scaffold assembly dynamics. We propose that centrioles generate a local pulse of Polo activity prior to mitotic entry to initiate centrosome maturation, explaining why centrioles and Polo/PLK1 are normally essential for this process.

Introduction

Centrosomes are important organisers of the cell that are formed when mother centrioles recruit a matrix of pericentriolar material (PCM) around themselves (Conduit *et al*, 2015; Bornens, 2021; Vasquez-Limeta & Loncarek, 2021; Lee *et al*, 2021; Woodruff, 2021). The PCM contains several hundred proteins (Alves-Cruzeiro *et al*, 2013), including many that help nucleate and organise microtubules (MTs), as well as many signalling molecules, cell cycle regulators, and checkpoint proteins. In this way, the centrosomes function as major MT organising centres (MTOC) and also important coordination centres in many cell types (Arquint *et al*, 2014; Chavali *et al*, 2014).

In interphase, most cells organise relatively little PCM, but there is a dramatic increase in PCM recruitment as cells prepare to enter mitosis—a process termed centrosome maturation (Palazzo *et al*, 2000; Conduit *et al*, 2015). Centrioles are required to initiate efficient mitotic PCM assembly (Bobinnec *et al*, 1998; Kirkham *et al*, 2003; Basto *et al*, 2006; Sir *et al*, 2013; Bazzi & Anderson, 2014; Wong *et al*, 2015), and, in worm embryos, centrioles are continuously required to promote the growth of the mitotic PCM—although they are not required to maintain the mitotic PCM once it has reached its full size in mitosis (Cabral *et al*, 2019).

The protein kinase Polo/PLK1 is also required for the assembly of the mitotic PCM in many, if not all, systems (Sunkel & Glover, 1988; Lane & Nigg, 1996; Dobbelaere *et al*, 2008; Haren *et al*, 2009; Lee & Rhee, 2011; Conduit *et al*, 2014a; Woodruff *et al*, 2015b; Ohta *et al*, 2021). PLK1 performs many functions during mitosis (Archambault & Glover,

2009; Colicino & Hehnly, 2018), and it is recruited to different locations within the cell via its Polo-Box-Domain (PBD), which binds to phosphorylated S-S(P)/T(P) motifs on various scaffolding proteins (Elia *et al*, 2003; Reynolds & Ohkura, 2003; Song *et al*, 2000; Seong *et al*, 2002). Importantly, PBD binding to these scaffolding proteins helps to activate PLK1 by relieving an inhibitory interaction between the PBD and the kinase domain (Xu *et al*, 2013). PLK1 is recruited to centrosomes by the scaffolding protein CEP192 in vertebrates (Joukov *et al*, 2010, 2014; Meng *et al*, 2015), and by the CEP192 homologues Spd-2/SPD-2 in flies and worms (Decker *et al*, 2011; Alvarez-Rodrigo *et al*, 2019; Ohta *et al*, 2021). In these species, the Polo/PLK-1 recruited by Spd-2/SPD-2 can then phosphorylate Cnn/SPD-5 (flies/worms), which allows these large helical proteins to assemble into macromolecular PCM-scaffolds that help recruit the many other PCM "client" proteins (Conduit *et al*, 2014a; Woodruff *et al*, 2015a; Feng *et al*, 2017; Woodruff *et al*, 2017; Cabral *et al*, 2019; Ohta *et al*, 2021).

Here, we measure the kinetics of mitotic PCM scaffold assembly in living *Drosophila* syncytial blastoderm embryos—where we can simultaneously track the behaviour of tens to hundreds of centrosomes as they rapidly and near-synchronously proceed through several rounds of mitosis in a common cytoplasm. Surprisingly, we observe that the centrosomal levels of Polo rise and fall during the centrosome assembly process, with centrosomal levels peaking, and then starting to decline, even as the Cnn scaffold continues to grow. Mathematical modelling and further experiments indicate that an interaction between Polo and its centriole receptor Ana1 (CEP295 in vertebrates) could generate a local pulse of centriolar Polo activity, and that such a mechanism could explain

the unexpected assembly kinetics of the PCM scaffold. We propose that centrioles generate a local pulse of Polo activity that initiates mitotic centrosome growth in syncytial fly embryos. We speculate that this may be a conserved feature of the assembly process, explaining why centrioles and Polo/PLK1 are normally required to initiate the efficient assembly of the mitotic PCM.

Results

PCM-scaffold proteins exhibit distinct assembly dynamics

To better understand how Spd-2, Polo and Cnn cooperate to assemble the PCM scaffold we quantified their recruitment dynamics in syncytial *Drosophila* embryos during nuclear cycles 11-13 (Figure 1). In the experiments reported here we used fluorescent reporters fused to several different fluorescent tags—Neon Green (NG), GFP, RFP or mCherry—(see Table 2, Materials and Methods). Expression levels of the Spd-2- and Cnn-fusion proteins used to measure recruitment dynamics were similar to endogenous levels (Figure S1), while the Polo-GFP fusion was expressed from a GFP-insertion into the endogenous Polo gene (Buszczak *et al*, 2007).

The rapid nuclear cycles in these embryos comprise alternating periods of S- and M-phase without intervening Gap periods, and S-phase gradually lengthens at each successive cycle (Foe & Alberts, 1983). As expected, the centrosomal levels of NG-Cnn increased through most of S-phase in all of the nuclear cycles, as this is the period when centrosomes grow in preparation for mitosis in these rapidly cycling embryos. In cycle 11, NG-Cnn levels continued to increase after the embryos had entered mitosis, which was scored by nuclear envelope breakdown (NEB; t=0 in Figure 1A; mitosis is indicated by the *grey shading* in the graphs in Figure 1A). In cycles 12 and 13 centrosomal levels of NG-Cnn peaked and then largely plateaued at about the time (cycle 12), or a few minutes before (cycle 13), the embryos entered mitosis. Perhaps surprisingly, the centrosomal levels of Spd-2-GFP and Polo-GFP did not increase throughout S-phase, but exhibited a pulsatile behaviour, with levels peaking in mid-late S-phase and then starting to decline

well before NEB (Figure 1A). In these syncytial embryos, S-phase length is determined by the activity of the core Cdk/Cyclin **c**ell **c**ycle **o**scillator (CCO) that drives progression through these early nuclear cycles (Farrell & O'Farrell, 2014; Liu *et al*, 2021). There was a strong correlation ($r\sim0.96$; $p<0.0001$) between S-phase length and the time at which Spd-2 and Polo levels peaked (Figure 1B), indicating that the CCO is likely to influence the period of the pulse of centrosomal Polo and Spd-2 recruitment.

In early *Drosophila* embryos, Spd-2 is thought to be the major protein that recruits Polo into the assembling mitotic PCM (Alvarez-Rodrigo *et al*, 2019), but the shapes of the Spd-2 and Polo centrosomal recruitment curves were quite distinct (Figure 1A). Surprisingly, during each cycle centrosomal Polo levels appeared to peak slightly before Spd-2 levels peaked, while the centrosomal levels of both Polo and Spd-2 peaked before the levels of Cnn peaked—meaning that the Cnn scaffold could continue to grow or plateau even as the centrosomal levels of Polo and Spd-2 declined (Figure 1A). As these measurements were taken from different sets of embryos expressing each protein individually, we confirmed these relative timings in embryos co-expressing Spd-2-mCherry with either Polo-GFP or GFP-Cnn (Figure 1C,D).

An underlying pulse of Polo activity could explain the observed kinetics of PCM scaffold assembly

As the rise and fall in centrosomal Polo levels appeared to precede the rise and fall in centrosomal Spd-2 levels (Figure 1D), we wondered whether the centrosomes might generate a pulse of Polo activity to initiate the assembly of the mitotic PCM scaffold. We

have previously developed a molecular model to explain how Spd-2, Polo and Cnn cooperate to assemble the mitotic PCM scaffold in flies (Figure 2A). In this scheme, Spd-2 is phosphorylated at centrioles as cells prepare to enter mitosis allowing Spd-2 to form a scaffold that fluxes outwards away from the centriole (Conduit *et al*, 2014b). This scaffold is structurally weak, but it can bind Polo and Cnn from the cytoplasm, which stabilises the scaffold (indicated by the *dotted line* in Figure 2A). This pool of Polo can then phosphorylate the Cnn to generate an independent Cnn scaffold which is structurally strong and can flux outwards from the Spd-2 scaffold along the centrosomal MTs (Conduit *et al*, 2014a; Feng *et al*, 2017) (see Figure S2 for a cartoon illustration of this scheme).

We turned to mathematical modelling to test whether imposing an underlying pulse of centriolar Polo activity on these proposed molecular interactions could explain the observed kinetics of PCM scaffold assembly. In this model (*Model* 1; Figure 2B) we assume that a pulse of active Polo (P^*) is generated at the surface of mother centrioles, with levels peaking at mid-S-phase (we explore later how this pulse might be generated). We allow centrosomal receptors (R_S) to recruit cytoplasmic Spd-2 (S) to the centriole to form the complex $\bar{R}_S$. The Spd-2 bound to this complex can be phosphorylated by P^* and converted to a form that can form a scaffold (S^*) that is released from $\bar{R}_S$ to flux outwards. This scaffold is unstable and can be rapidly converted back to S by a phosphatase, which we allow to be active in the cytoplasm at a constant level. However, S^* can also bind cytoplasmic Polo (P) and Cnn (C) to form a more stable scaffold ($\bar{S}$) that converts back to S relatively slowly. When bound to $\bar{S}$, Polo is activated so that it can phosphorylate the $\bar{S}$-bound Cnn and convert it into a form (C^*) that can form a scaffold and be released from

$\bar{S}$ to flux further outwards. In this way, the Spd-2 scaffold acts to convert catalytically C into the scaffold C^*. The C^* scaffold disassembles when it is dephosphorylated by a cytoplasmic phosphatase, which we allow to be active in the cytoplasm at a constant level. We also allow the rate of C^* disassembly to increase as the size of the C^* scaffold increases, which appears to be the case in these embryos (Conduit *et al*, 2010).

We modelled these reactions as a system of ordinary differential equations (ODEs, detailed in Materials and Methods) and studied the behaviour of the system. Encouragingly, this model recapitulated two of the most surprising features of scaffold assembly dynamics that we observed *in vivo* (Figure 2C): (1) The imposed centriolar P^* pulse (*solid green line*, Figure 2B) generated a subsequent pulse in centrosomal Spd-2 levels (*dotted orange line*, Figure 2C); (2) the system generated the assembly of a Cnn scaffold (*dotted blue line*, Figure 2C) that could continue to grow and then plateau even as centrosomal Polo and Spd-2 levels declined. Thus, this simple molecular model, when combined with an imposed pulse of centriolar Polo activity, can explain the basic dynamic features of PCM scaffold assembly kinetics that we observe *in vivo*.

Spd-2 and Ana1 help to generate the centrosomal Polo pulse

How might the centrioles generate a pulse of Polo activity? This pulse of activity is unlikely to simply reflect the general activity of Polo in the embryo, which, like Cdk/Cyclin activity (Deneke *et al*, 2016), peaks during mitosis (Stefano Di Talia, Duke University (USA), *personal communication*). Thus, the centrioles must generate a local pulse of Polo activity well before Polo is maximally activated in the rest of the embryo more generally.

Polo/PLK1 is known to be recruited to mitotic centrosomes by its Polo-box domain (PBD) that binds to phosphorylated S-S(P)/T(P) motifs (Elia *et al*, 2003; Reynolds & Ohkura, 2003; Song *et al*, 2000; Seong *et al*, 2002); this recruitment is sufficient to at least partially activate the kinase (Xu *et al*, 2013). In fly embryos, the Polo required for mitotic PCM assembly appears to be recruited to centrosomes via the sequential phosphorylation of S-S(P)/T(P) motifs first in Ana1 (that recruits Polo to mother centrioles) (Alvarez-Rodrigo *et al*, 2021) and then in Spd-2 (which recruits Polo into the expanding mitotic PCM) (Alvarez-Rodrigo *et al*, 2019).

To test the potential role of these proteins in generating the Polo pulse we examined Polo-GFP recruitment during nuclear cycle 12 in embryos expressing a mutant form of either Ana1 (Ana1-S34T-mCherry) (Alvarez-Rodrigo *et al*, 2021) or Spd-2 (Spd-2-S16T-mCherry—previously called Spd-2-CONS-mCherry) (Alvarez-Rodrigo *et al*, 2019) in which multiple S-S/T motifs (34 for Ana1 and 16 for Spd-2) were mutated to T-S/T (Figure 3). These conservative substitutions severely impair the ability of the mutant proteins to recruit Polo, seemingly without perturbing other aspects of their function (Alvarez-Rodrigo *et al*, 2019, 2021). These experiments were performed in the presence of endogenous, untagged, Spd-2 or Ana1 because embryos laid by females co-expressing Polo-GFP in the presence of only Ana1-S34T or Spd-2-S16T die very early in development due to centrosome defects (Alvarez-Rodrigo *et al*, 2019, 2021)—as centrosomes are essential for early embryo development (Stevens *et al*, 2007; Varmark *et al*, 2007), but not for the rest of development in *Drosophila* (Basto *et al*, 2006).

In these experiments, we examined the centrosomes organised by the old-mother centriole (hereafter OM centrosomes) and new-mother centriole (hereafter NM centrosomes) separately, as they behaved differently. In embryos expressing Polo-GFP and WT-Ana1-mCherry, the Polo pulse was similar on OM and NM centrosomes, although NM centrosomes initially organised significantly less Polo than OM centrosomes (Figure 3A,B). This is because at the start of S-phase NMs are recruiting Polo for the first time, whereas OMs retain some of the mitotic PCM that they had recruited in the previous cycle (Conduit *et al*, 2010). In embryos expressing Polo-GFP and Ana1-S34T-mCherry, the Polo pulse was relatively normal on OMs—although the amplitude was slightly increased (the potential reasons for this are discussed in the last Results Section)—but it was dramatically perturbed on NMs, exhibiting a reduced growth rate, a lower amplitude and a longer period (Figure 3A,B). Ana1-S34T probably preferentially perturbs NM centrosomes because Ana1 is only required to recruit Polo to the mother centrioles (not to the PCM), and we showed previously that once some mitotic PCM has been established around a centriole (as is the case at OM centrosomes), it can help recruit Polo to centrosomes and so partially bypass the requirement for Ana1 to initially recruit Polo to the centriole (Alvarez-Rodrigo *et al*, 2021).

The Polo-GFP pulse was relatively normal on OM and NM centrosomes in embryos co-expressing WT Spd-2-mCherry, but was dramatically perturbed in embryos expressing Spd-2-S16T-mCherry—exhibiting a reduced growth rate, a lower amplitude and a longer period (Figure 3C,D). In contrast to Ana1-S34T, however, the Polo-GFP pulse was equally perturbed on both OM and NM centrosomes in the presence of Spd-2-S16T. This

is probably due to the fact that Spd-2 is primarily responsible for recruiting Polo-GFP to the mitotic PCM (rather than to the centrioles), so OM centrosomes cannot eventually establish a relatively normal mitotic PCM in the presence of Spd-2-S16T. Taken together, these results indicate that Ana1 and Spd-2 play an important part in generating the centrosomal Polo pulse, with Ana1 having the dominant role in initially recruiting Polo to the centrioles and Spd-2 having the dominant role in subsequently recruiting Polo to the expanding mitotic PCM.

Mathematical modelling indicates that an interaction between Ana1 and Polo could generate a centrosomal pulse of Polo activity

We noticed that expressing either Ana1-S34T or Spd-2-S16T in embryos perturbed not only the amplitude of the Polo pulse, but also its period (Figure 3). Moreover, in embryos expressing Ana1-S34T the period was significantly perturbed on NM centrosomes but not on OM centrosomes—even though these centrosomes co-exist in the same cytoplasm. This suggests that the kinetics of the Polo pulse are generated by mechanisms that act locally on individual centrosomes (rather than globally on the embryo as a whole), and that the Polo recruited to each centriole might have a role in inactivating the ability of that centrosome to recruit more Polo—as in Ana1-S34T embryos the OM centrosomes (that have high levels of Polo) appear to stop recruiting Polo before NM centrosomes (that have lower levels of Polo) (Figure 3A,B). With this in mind, we developed a simple mathematical model to explain how the interaction between Polo (*P*) and its centriolar Receptor (R_P) (in these embryos most likely Ana1) might generate a pulse of Polo activity.

In this model (*Model 2*; Figure 4A), the centriolar Polo receptor is initially in an inactive state that cannot recruit Polo (R_P^{off}). Mitotic PCM recruitment is initiated when R_P^{off} is phosphorylated on S-S(P)/T(P) motifs by a kinase to generate R_P. These activated receptors can recruit and activate cytoplasmic Polo to form the complex $\bar{R}_{P^*}$. This pool of centriole-bound active Polo can phosphorylate the Spd-2 bound to the centriolar Receptor complex $\bar{R}_S$—also potentially Ana1/CEP295 (Tsuchiya *et al*, 2016)—to generate S^*. This initiates mitotic PCM scaffold assembly (as described in *Model 1*; Figure 2A). Crucially, we also allow the centriole-bound active Polo to slowly phosphorylate $\bar{R}_{P^*}$ at additional sites (i.e. not the original S-S/T motifs) to generate $\bar{R}_P^{\text{off}}$, which can no longer recruit Polo. In this way, an activator (R_P), activates its own inhibitor (P^*) to form a classical delayed negative feedback network (Novák & Tyson, 2008), which generates a local pulse of Polo activity at the centriole (*dotted green* line, Figure 4B). We speculate that this system is reset at the end of each nuclear cycle when $\bar{R}_P^{\text{off}}$ is dephosphorylated during mitosis by a phosphatase to regenerate R_P^{off} (this step is not depicted in the schematic, Figure 4A, and we do not model it here). When we used the pulse of Polo activity generated by *Model 2* to feed into *Model 1* to generate the PCM scaffold, it produced assembly kinetics that were similar to the original *Model 1* (where we simply imposed a Polo pulse on the system) (Figure 4B). Hence, *Model 2* provides a plausible mechanism to explain how centrioles might generate a pulse of Polo activity.

As Polo/PLK1 turns over rapidly at centrosomes (Kishi *et al*, 2009; Mahen *et al*, 2011) (see also below), the centrosomal Polo receptors (Ana1 and Spd-2) may constantly generate and then release active Polo, which could diffuse and phosphorylate local

targets before it is inactivated. Such a scenario, depicted in *Model 3* (Figure 4C), also generated PCM scaffold assembly kinetics that were similar to the original *Model 1* (Figure 4D). Importantly, this model provides an intuitive explanation as to why reducing the ability of centrosomes to recruit Polo (for example, by expressing either Ana1-S34T or Spd-2-S16T) lengthens the period of the Polo pulse (Figure 3). If the centriole and PCM receptors (Ana1 and Spd-2, respectively) recruit less Polo, the centriole receptor (Ana1) will be inactivated more slowly. Thus, in the presence of Spd-2-S16T or Ana1-S34T, Polo would be recruited more slowly, but for a longer period—as we observe (Figure 3).

The rate of Polo recruitment and PCM scaffold growth is influenced by the Cdk/Cyclin cell cycle oscillator (CCO)

As described above, the period of the centrosomal pulse of Polo recruitment is strongly correlated with S-phase length (Figure 1B), which is determined by CCO activity (Farrell & O'Farrell, 2014; Liu *et al*, 2021). We speculate that in our molecular model the CCO could influence Polo recruitment by regulating the rate (k_R^{on}) at which the centriolar Polo receptor (likely Ana1) is phosphorylated (Figure 4A,C). If this receptor is initially phosphorylated more slowly, then Polo will be recruited more slowly and the PCM scaffold will grow more slowly. During nuclear cycles 10-13, the rate at which the CCO is activated during S-phase naturally slows at successive cycles (Farrell & O'Farrell, 2014; Liu *et al*, 2021). Thus, if our model is correct, the rate of Polo recruitment to the centrosome should slow at each successive nuclear cycle, and the rate of Spd-2 and Cnn scaffold growth should also slow. To test if this was the case we performed a Fluorescence Recovery After Photobleaching (FRAP) analysis (Figure 5; Figure S3). The fluorescent signal of the

three PCM scaffold proteins recovered at very different rates (note the different timescales in Figure 5A-C) with Polo turning over with a $t_{1/2}$ of ~10secs and Spd-2 and Cnn fluorescence recovering more slowly. Strikingly, however, the average rate of fluorescence recovery of all three proteins slowed at successive cycles (Figure 5B), consistent with our hypothesis that these parameters are influenced by the CCO.

In interpreting this experiment it is important to remember that Spd-2 and Cnn do not "turn-over" at centrosomes in the classical sense, as both proteins incorporate into the PCM in the central region around the mother centriole and then flux outwards to leave the PCM from the more peripheral regions (Conduit *et al*, 2010, 2014b). Thus, the initial rate of fluorescence "recovery" that we measure for Spd-2 and Cnn largely reflects the growth of the scaffold (i.e. the incorporation of new Spd-2 and Cnn molecules into the central region) rather than the turn-over of molecules already incorporated into the PCM. This is not the case for Polo, which turns-over rapidly throughout the entire PCM volume as it binds and unbinds from its centrosomal receptors (Conduit *et al*, 2014b). Thus, we believe the decreased rate of Polo turnover at centrosomes at successive cycles reflects the slowing rate at which its receptors are activated by the CCO at successive cycles, while the decreasing rate of Spd-2 and Cnn addition at successive cycles reflects the slower growth of the scaffold caused by the slower recruitment of Polo.

<u>Mathematical modelling predicts the consequence of lowering the concentration of either Spd-2 or Ana1</u>

To test whether our mathematical models have predictive power, we used them to model the consequences of halving the amount of either Spd-2 or Ana1 in the system, while we measured experimentally the Polo-GFP pulse in embryos laid by females expressing only one copy of *Spd-2* (*Spd-2*$^{+/-}$ embryos) or *ana1* (*ana1*$^{+/-}$ embryos) (Figure 6). Although the precise shape of the growth curves generated by the mathematical model (Figure 6A,C) did not match closely the experimental data (Figure 6B,D) (the reasons for this are discussed below), the model correctly predicted that halving Spd-2 levels would lead to a general reduction in centrosomal Polo recruitment (Figure 6A). Perhaps more convincingly, the model also correctly predicted the non-intuitive observation that although halving Ana1 levels led to an initial reduction in centrosomal Polo levels, the centrosomes in the *ana1*$^{+/-}$ embryos ultimately associated with *more* Polo than controls by the end of S-phase (Figure 6B). In our model, this occurs because the peak of the Polo pulse is shifted to later in S-phase and its rate of decline is shallower in the half-dose *ana1*$^{+/-}$ embryos—because the Ana1 Polo receptors are inactivated more slowly. This may also explain why OM centrosomes, that have recruited Polo during the previous cycle, seem to recruit more Polo than normal if they express some Ana1-S34T protein (Figure 3A). Thus, our mathematical model can make useful and non-intuitive predictions about the broad behaviour of the PCM scaffold system.

We note that our mathematical models are purposefully minimal to reduce the number of parameters and test possible mechanisms rather than to mimic experimental data. This approach explains why the overall shape of the predicted growth curves do not exhibit all of the finer characteristics of the experimental data. For instance, in our models the Polo

and Spd-2 pulses consistently have higher amplitudes and earlier peaks compared to experimental data (see, for example, Figure 6). In principle, this problem can be solved by introducing additional intermediate steps into the model (e.g. by requiring that the centriolar receptors are phosphorylated on multiple sites to be activated). Any such additional steps will delay the system (and so shift the peaks to later in S-phase), and also allow the receptors to simultaneously occupy a larger distribution of states (and so dampen the amplitude). Since such intermediate states are likely to exist—Ana1 and Spd-2, for example, both appear to be phosphorylated on multiple sites to recruit Polo (Alvarez-Rodrigo *et al*, 2019, 2021)—we acknowledge the consequences of neglecting them in our model but choose to do so in favour of simplicity.

Discussion

We show here that the mother centrioles in the early *Drosophila* embryo generate a pulse of Polo activity at the start of each nuclear cycle, and we propose that this initiates centrosome maturation by catalysing the local assembly of a Spd-2/Cnn PCM scaffold around the mother centriole. In the early *Drosophil*a embryo, the global cytoplasmic activity of mitotic kinases such as Cdk1 and Polo are relatively low at the start of each nuclear cycle, but they rise steadily to peak during mitosis (Deneke *et al*, 2016) (Stefano Di Talia, personal communication). Thus, the local activation of Polo at centrioles precedes, and is likely to be independent of, the global rise in Polo activity that occurs in the embryo more generally. Recent experiments suggest that a similar mechanism operates in the early *C. elegans* embryo. These embryos build a mitotic PCM scaffold using a PLK-1/SPD-2/SPD-5 system that is analogous to the Polo/Spd-2/Cnn system in fly embryos (Hamill *et al*, 2002; Kemp *et al*, 2004; Pelletier *et al*, 2004; Dammermann *et al*, 2004; Woodruff *et al*, 2015a; Laos *et al*, 2015; Wueseke *et al*, 2016; Magescas *et al*, 2019; Ohta *et al*, 2021). In these embryos, the centrioles and PLK-1 are continuously required to promote the growth of the mitotic PCM (Cabral *et al*, 2019), indicating that, as in fly embryos, the centrioles provide a source of Polo/PLK-1 activity that initiates and sustains the growth of the mitotic centrosome prior to mitotic entry (Zwicker *et al*, 2014; Cabral *et al*, 2019).

We speculate that this mechanism may be a common feature of centrosome maturation in many cell types, not just embryos. In many cells, the centrosomes start to mature prior to NEB, so presumably well before Polo is fully activated in the cytoplasm. In these

systems, mother centrioles could initiate centrosome maturation by locally activating Polo/PLK1 prior to mitosis, which would explain why the centrioles and Polo/PLK1 kinases appear to be required to initiate the efficient assembly of the mitotic PCM in many systems. Once cells are in mitosis, however, the high levels of active Polo/PLK1 in the cytoplasm may be sufficient to sustain the assembled mitotic PCM and centrioles may no longer be required. This is the case in worm embryos, where centrioles are not required to maintain the fully grown mitotic PCM during mitosis—although PLK-1 activity is still required, and is presumably provided from the cytoplasm (Cabral *et al*, 2019).

Although high levels of centrosomal Polo/PLK1 may not be required to sustain the mitotic PCM once cells are in mitosis, centrosomal levels of PLK1 nevertheless remain relatively high during mitosis in human cells and worm embryos and only rapidly decline as cells exit mitosis (Golsteyn *et al*, 1995; Mittasch *et al*, 2020). It is therefore unclear why Polo levels start to decrease prior to the entry into mitosis in *Drosophila* embryos. A possible explanation is that in these rapidly cycling embryos the mitotic PCM has to be disassembled very quickly at the end of mitosis, as there are just a few minutes before the next cycle of assembly begins. The early disassembly of the Spd-2/Polo scaffold might be important to allow the subsequent rapid disassembly of the remaining mitotic PCM. Interestingly, PLK-1 also appears to be the first mitotic PCM component to start leaving the centrosome in worm embryos—although it only does so at the end of mitosis (Mittasch *et al*, 2020). In summary, although the molecular details and precise timing will vary, the ability of centrioles to switch-on, and then switch-off, the local activation of

Polo/PLK1 kinase may be a common feature of mitotic centrosome assembly and disassembly in many different cell types.

Our data and mathematical modelling are consistent with the possibility that Polo is recruited and activated at centrioles to initiate mitotic PCM assembly in fly embryos by its interactions with Ana1 and Spd-2. PLK1 binding to phosphorylated S-S(P)/T(P) motifs activates its kinase activity (Xu *et al*, 2013), and we have previously shown that in flies at least three proteins can recruit Polo to centrioles via these motifs: Sas-4 (Novak *et al*, 2016), Ana1 (Alvarez-Rodrigo *et al*, 2021) and Spd-2 (Alvarez-Rodrigo *et al*, 2019)—with the latter two proteins having roles in recruiting Polo specifically to promote centrosome maturation. Spd-2/SPD-2/CEP192 proteins appear to be universally required for mitotic centrosome assembly (Kemp *et al*, 2004; Pelletier *et al*, 2004; Gomez-Ferreria *et al*, 2007; Zhu *et al*, 2008; Dix & Raff, 2007; Giansanti *et al*, 2008), and their ability to help recruit Polo/PLK-1/PLK1 to centrosomes is highly conserved (Decker *et al*, 2011; Joukov *et al*, 2014; Meng *et al*, 2015; Alvarez-Rodrigo *et al*, 2019). Worms do not have an obvious Ana1 homologue—although proteins such as SAS-7 (Sugioka *et al*, 2017) or PCMD-1 (Stenzel *et al*, 2021) could perform an analogous function—but in both flies and humans Ana1/CEP295 proteins are required to allow centrioles to recruit mitotic PCM (Izquierdo *et al*, 2014; Fu *et al*, 2016; Tsuchiya *et al*, 2016; Saurya *et al*, 2016). Thus, it seems likely that at least elements of the fly system that generates the Polo pulse will be conserved. It will be important to determine whether CEP295 helps to recruit PLK1 to centrioles in human cells.

Finally, our studies reveal interesting similarities between the proposed mechanisms that regulate the growth of the daughter centriole (Aydogan *et al*, 2018, 2020) and the growth of the mitotic PCM. In both cases, centrioles organise a local pulse in the activity of a key enzyme (Plk4 or Polo/PLK1) that regulates the incorporation of key building blocks (Ana2/Sas-6 or Spd-2/Cnn) into an organelle scaffolding structure (the centriole cartwheel or the mitotic PCM scaffold). Moreover, both systems are normally entrained in the embryo by the core CCO to ensure that organelle assembly not only occurs in the right place, but also at the right time. Could similar principles regulate the growth of other organelles? It is becoming clear that the biogenesis of several membrane bound organelles occurs primarily at specialised membrane contact sites where key activities are concentrated (Wu *et al*, 2018; Farré *et al*, 2019; Prinz *et al*, 2020). It will be interesting to determine if these key activities are recruited to these sites in a pulsatile fashion, and, if so, whether these activity pulses are entrained by master oscillators such as the CCO and/or the circadian clock to ensure that organelle biogenesis not only occurs at the right place, but also at the appropriate time.

Acknowledgements

We are grateful to Lisa Gartenmann for generating the Ubq-NG-Cnn line, and to Alan Wainman for help with microscopy as part of the Micron Oxford Advanced Bioimaging Unit—partly funded by a Strategic Award from the Wellcome Trust (107457). We thank members of the Raff Laboratory for advice, discussion and for critically reading the manuscript. The research was funded by a Wellcome Trust Senior Investigator Award (215523) to J.W.R., an EPSRC award (EP/R020205/1) and a John Fell Fund Award to A.G., and a CRUK Oxford Centre Prize DPhil Studentship (C5255/A23225), a Balliol Jason Hu Scholarship and a Clarendon Scholarship (to S.S.W.).

Author contributions

This study was conceptualised by S.S.W., Z.M.W., A.G., and J.W.R. Investigation was done by S.S.W. and Z.M.W. Key reagents were generated by S.S. Computational analysis pipelines were developed by S.S.W., K.Y.C. and F.Y.Z. Data was analysed by S.S.W., Z.M.W., A.G., and J.W.R. The project was supervised and administered by A.G. and J.W.R. The manuscript was initially drafted by S.S.W., Z.M.W., A.G., and J.W.R. and all authors contributed to the editing of the manuscript.

Declaration of interests

The authors declare no competing interests.

References

Alvarez-Rodrigo I, Steinacker TL, Saurya S, Conduit PT, Baumbach J, Novak ZA, Aydogan MG, Wainman A & Raff JW (2019) Evidence that a positive feedback loop drives centrosome maturation in fly embryos. *eLife* 8

Alvarez-Rodrigo I, Wainman A, Saurya S & Raff JW (2021) Ana1 helps recruit Polo to centrioles to promote mitotic PCM assembly and centriole elongation. *Journal of Cell Science* 134

Alves-Cruzeiro JM da C, Nogales-Cadenas R & Pascual-Montano AD (2013) CentrosomeDB: a new generation of the centrosomal proteins database for Human and Drosophila melanogaster. *Nucleic Acids Research* 42: D430-6

Archambault V & Glover DM (2009) Polo-like kinases: conservation and divergence in their functions and regulation. *Nat Rev Mol Cell Biol* 10: 265–275

Arquint C, Gabryjonczyk A-M & Nigg EA (2014) Centrosomes as signalling centres. *Curr Biol* 369: 20130464–20130464

Aydogan MG, Steinacker TL, Mofatteh M, Wilmott ZM, Zhou FY, Gartenmann L, Wainman A, Saurya S, Novak ZA, Wong S-S, *et al* (2020) An Autonomous Oscillation Times and Executes Centriole Biogenesis. *Cell* 181: 1566-1581.e27

Aydogan MG, Wainman A, Saurya S, Steinacker TL, Caballe A, Novak ZA, Baumbach J, Muschalik N & Raff JW (2018) A homeostatic clock sets daughter centriole size in flies. *J Cell Biol* 217: 1233–1248

Basto R, Lau J, Vinogradova T, Gardiol A, Woods CG, Khodjakov A & Raff JW (2006) Flies without centrioles. *Cell* 125: 1375–1386

Bazzi H & Anderson KV (2014) Acentriolar mitosis activates a p53-dependent apoptosis pathway in the mouse embryo. *Proc Natl Acad Sci USA* 111: E1491-500

Bobinnec Y, Khodjakov A, Mir LM, Rieder CL, Eddé B & Bornens M (1998) Centriole disassembly in vivo and its effect on centrosome structure and function in vertebrate cells. *J Cell Biol* 143: 1575–1589

Bornens M (2021) Centrosome organization and functions. *Curr Opin Struct Biol* 66: 199–206

Buszczak M, Paterno S, Lighthouse D, Bachman J, Planck J, Owen S, Skora AD, Nystul TG, Ohlstein B, Allen A, *et al* (2007) The Carnegie Protein Trap Library: A Versatile Tool for Drosophila Developmental Studies. *Genetics* 175: 1505–1531

Cabral G, Laos T, Dumont J & Dammermann A (2019) Differential requirements for centrioles in mitotic centrosome growth and maintenance. *Developmental Cell* 50: 355-366.e6

Chavali PL, Putz M & Gergely F (2014) Small organelle, big responsibility: the role of centrosomes in development and disease. *Philosophical Transactions of the Royal Society B: Biological Sciences* 369: 20130468–20130468

Colicino EG & Hehnly H (2018) Regulating a key mitotic regulator, polo-like kinase 1 (PLK1). *Cytoskeleton (Hoboken)* 75: 481–494

Conduit PT, Brunk K, Dobbelaere J, Dix CI, Lucas EP & Raff JW (2010) Centrioles regulate centrosome size by controlling the rate of Cnn incorporation into the PCM. *Curr Biol* 20: 2178–2186

Conduit PT, Feng Z, Richens JH, Baumbach J, Wainman A, Bakshi SD, Dobbelaere J, Johnson S, Lea SM & Raff JW (2014a) The centrosome-specific phosphorylation of Cnn by Polo/Plk1 drives Cnn scaffold assembly and centrosome maturation. *Developmental Cell* 28: 659–669

Conduit PT, Richens JH, Wainman A, Holder J, Vicente CC, Pratt MB, Dix CI, Novak ZA, Dobbie IM, Schermelleh L, *et al* (2014b) A molecular mechanism of mitotic centrosome assembly in Drosophila. *Elife* 3: e03399

Conduit PT, Wainman A & Raff JW (2015) Centrosome function and assembly in animal cells. *Nature Reviews Molecular Cell Biology* 16: 611–624

Dammermann A, Müller-Reichert T, Pelletier L, Habermann B, Desai A & Oegema K (2004) Centriole assembly requires both centriolar and pericentriolar material proteins. *Dev Cell* 7: 815–829

Decker M, Jaensch S, Pozniakovsky A, Zinke A, O'Connell KF, Zachariae W, Myers E & Hyman AA (2011) Limiting amounts of centrosome material set centrosome size in C. elegans embryos. *Current Biology* 21: 1259–1267

Deneke VE, Melbinger A, Vergassola M & Di Talia S (2016) Waves of Cdk1 Activity in S Phase Synchronize the Cell Cycle in Drosophila Embryos. *Dev Cell* 38: 399–412

Dix CI & Raff JW (2007) Drosophila Spd-2 recruits PCM to the sperm centriole, but is dispensable for centriole duplication. *Curr Biol* 17: 1759–1764

Dobbelaere J, Josué F, Suijkerbuijk S, Baum B, Tapon N & Raff JW (2008) A genome-wide RNAi screen to dissect centriole duplication and centrosome maturation in Drosophila. *PLoS Biology* 6: e224

Elia AEH, Rellos P, Haire LF, Chao JW, Ivins FJ, Hoepker K, Mohammad D, Cantley LC, Smerdon SJ & Yaffe MB (2003) The molecular basis for phosphodependent substrate targeting and regulation of Plks by the Polo-box domain. *Cell* 115: 83–95

Farré J-C, Mahalingam SS, Proietto M & Subramani S (2019) Peroxisome biogenesis, membrane contact sites, and quality control. *EMBO Rep* 20

Farrell JA & O'Farrell PH (2014) From egg to gastrula: how the cell cycle is remodeled during the Drosophila mid-blastula transition. *Annu Rev Genet* 48: 269–294

Feng Z, Caballe A, Wainman A, Johnson S, Haensele AFM, Cottee MA, Conduit PT, Lea SM & Raff JW (2017) Structural basis for mitotic centrosome assembly in flies. *Cell* 169: 1078-1089.e13

Foe VE & Alberts BM (1983) Studies of nuclear and cytoplasmic behaviour during the five mitotic cycles that precede gastrulation in Drosophila embryogenesis. *J Cell Sci* 61: 31–70

Fu J, Lipinszki Z, Rangone H, Min M, Mykura C, Chao-Chu J, Schneider S, Dzhindzhev NS, Gottardo M, Riparbelli MG, *et al* (2016) Conserved molecular interactions in centriole-to-centrosome conversion. *Nat Cell Biol* 18: 87–99

Giansanti MG, Bucciarelli E, Bonaccorsi S & Gatti M (2008) Drosophila SPD-2 is an essential centriole component required for PCM recruitment and astral-microtubule nucleation. 18: 303–309

Golsteyn RM, Mundt KE, Fry AM & Nigg EA (1995) Cell cycle regulation of the activity and subcellular localization of Plk1, a human protein kinase implicated in mitotic spindle function. *Journal of Cell Biology* 129: 1617–1628

Gomez-Ferreria MA, Rath U, Buster DW, Chanda SK, Caldwell JS, Rines DR & Sharp DJ (2007) Human Cep192 is required for mitotic centrosome and spindle assembly. 17: 1960–1966

Hamill DR, Severson AF, Carter JC & Bowerman B (2002) Centrosome maturation and mitotic spindle assembly in C. elegans require SPD-5, a protein with multiple coiled-coil domains. *Dev Cell* 3: 673–684

Haren L, Stearns T & Lüders J (2009) Plk1-dependent recruitment of gamma-tubulin complexes to mitotic centrosomes involves multiple PCM components. *PLoS ONE* 4: e5976

Izquierdo D, Wang W-J, Uryu K & Tsou M-FB (2014) Stabilization of cartwheel-less centrioles for duplication requires CEP295-mediated centriole-to-centrosome conversion. *Cell Rep* 8: 957–965

Joukov V, De Nicolo A, Rodriguez A, Walter JC & Livingston DM (2010) Centrosomal protein of 192 kDa (Cep192) promotes centrosome-driven spindle assembly by engaging in organelle-specific Aurora A activation. *Proc Natl Acad Sci USA* 107: 21022–21027

Joukov V, Walter JC & De Nicolo A (2014) The Cep192-organized aurora A-Plk1 cascade is essential for centrosome cycle and bipolar spindle assembly. *Mol Cell* 55: 578–591

Kemp CA, Kopish KR, Zipperlen P, Ahringer J & O'Connell KF (2004) Centrosome maturation and duplication in C. elegans require the coiled-coil protein SPD-2. *Dev Cell* 6: 511–523

Kirkham M, Müller-Reichert T, Oegema K, Grill S & Hyman AA (2003) SAS-4 is a C. elegans centriolar protein that controls centrosome size. *Cell* 112: 575–587

Kishi K, van Vugt MATM, Okamoto K, Hayashi Y & Yaffe MB (2009) Functional Dynamics of Polo-Like Kinase 1 at the Centrosome. *Molecular and Cellular Biology* 29: 3134–3150

Lane HA & Nigg EA (1996) Antibody microinjection reveals an essential role for human polo-like kinase 1 (Plk1) in the functional maturation of mitotic centrosomes. *Journal of Cell Biology* 135: 1701–1713

Laos T, Cabral G & Dammermann A (2015) Isotropic incorporation of SPD-5 underlies centrosome assembly in C. elegans. *Curr Biol* 25: R648-9

Lee K & Rhee K (2011) PLK1 phosphorylation of pericentrin initiates centrosome maturation at the onset of mitosis. *J Cell Biol* 195: 1093–1101

Lee KS, Park J-E, Ahn JI & Zeng Y (2021) Constructing PCM with architecturally distinct higher-order assemblies. *Curr Opin Struct Biol* 66: 66–73

Liu B, Zhao H, Wu K & Großhans J (2021) Temporal Gradients Controlling Embryonic Cell Cycle. *Biology* 10: 513

Magescas J, Zonka JC & Feldman JL (2019) A two-step mechanism for the inactivation of microtubule organizing center function at the centrosome. *Elife* 8: e47867

Mahen R, Jeyasekharan AD, Barry NP & Venkitaraman AR (2011) Continuous polo-like kinase 1 activity regulates diffusion to maintain centrosome self-organization during mitosis. *Proc Natl Acad Sci USA* 108: 9310–9315

Meng L, Park J-E, Kim T-S, Lee EH, Park S-Y, Zhou M, Bang JK & Lee KS (2015) Bimodal Interaction of Mammalian Polo-Like Kinase 1 and a Centrosomal Scaffold, Cep192, in the Regulation of Bipolar Spindle Formation. *Mol Cell Biol* 35: 2626–2640

Mittasch M, Tran VM, Rios MU, Fritsch AW, Enos SJ, Ferreira Gomes B, Bond A, Kreysing M & Woodruff JB (2020) Regulated changes in material properties underlie centrosome disassembly during mitotic exit. *J Cell Biol* 219

Novák B & Tyson JJ (2008) Design principles of biochemical oscillators. *Nat Rev Mol Cell Biol* 9: 981–991

Novak ZA, Wainman A, Gartenmann L & Raff JW (2016) Cdk1 Phosphorylates Drosophila Sas-4 to Recruit Polo to Daughter Centrioles and Convert Them to Centrosomes. *Dev Cell* 37: 545–557

Ohta M, Zhao Z, Wu D, Wang S, Harrison JL, Gómez-Cavazos JS, Desai A & Oegema KF (2021) Polo-like kinase 1 independently controls microtubule-nucleating capacity and size of the centrosome. *J Cell Biol* 220

Palazzo RE, Vogel JM, Schnackenberg BJ, Hull DR & Wu X (2000) Centrosome maturation. *Curr Top Dev Biol* 49: 449–470

Pelletier L, Ozlü N, Hannak E, Cowan C, Habermann B, Ruer M, Müller-Reichert T & Hyman AA (2004) The Caenorhabditis elegans centrosomal protein SPD-2 is required for both pericentriolar material recruitment and centriole duplication. 14: 863–873

Prinz WA, Toulmay A & Balla T (2020) The functional universe of membrane contact sites. *Nat Rev Mol Cell Biol* 21: 7–24

Reynolds N & Ohkura H (2003) Polo boxes form a single functional domain that mediates interactions with multiple proteins in fission yeast polo kinase. *J Cell Sci* 116: 1377–1387

Saurya S, Roque H, Novak ZA, Wainman A, Aydogan MG, Volanakis A, Sieber B, Pinto DMS & Raff JW (2016) Drosophila Ana1 is required for centrosome assembly and centriole elongation. *J Cell Sci* 129: 2514–2525

Seong Y-S, Kamijo K, Lee J-S, Fernandez E, Kuriyama R, Miki T & Lee KS (2002) A spindle checkpoint arrest and a cytokinesis failure by the dominant-negative polo-box domain of Plk1 in U-2 OS cells. *J Biol Chem* 277: 32282–32293

Sir J-H, Pütz M, Daly O, Morrison CG, Dunning M, Kilmartin JV & Gergely F (2013) Loss of centrioles causes chromosomal instability in vertebrate somatic cells. *J Cell Biol* 203: 747–756

Song S, Grenfell TZ, Garfield S, Erikson RL & Lee KS (2000) Essential function of the polo box of Cdc5 in subcellular localization and induction of cytokinetic structures. *Mol Cell Biol* 20: 286–298

Stenzel L, Schreiner A, Zuccoli E, Üstüner S, Mehler J, Zanin E & Mikeladze-Dvali T (2021) PCMD-1 bridges the centrioles and the pericentriolar material scaffold in C. elegans. *Development* 148: dev198416

Stevens NR, Raposo AASF, Basto R, St Johnston D & Raff JW (2007) From stem cell to embryo without centrioles. *Current Biology* 17: 1498–1503

Sugioka K, Hamill DR, Lowry JB, McNeely ME, Enrick M, Richter AC, Kiebler LE, Priess JR & Bowerman B (2017) Centriolar SAS-7 acts upstream of SPD-2 to regulate centriole assembly and pericentriolar material formation. *Elife* 6: e20353

Sunkel CE & Glover DM (1988) polo, a mitotic mutant of Drosophila displaying abnormal spindle poles. *J Cell Sci* 89 (Pt 1): 25–38

Tsuchiya Y, Yoshiba S, Gupta A, Watanabe K & Kitagawa D (2016) Cep295 is a conserved scaffold protein required for generation of a bona fide mother centriole. *Nat Commun* 7: 12567

Varmark H, Llamazares S, Rebollo E, Lange B, Reina J, Schwarz H & González C (2007) Asterless is a centriolar protein required for centrosome function and embryo development in Drosophila. *Current Biology* 17: 1735–1745

Vasquez-Limeta A & Loncarek J (2021) Human centrosome organization and function in interphase and mitosis. *Semin Cell Dev Biol*

Wong YL, Anzola JV, Davis RL, Yoon M, Motamedi A, Kroll A, Seo CP, Hsia JE, Kim SK, Mitchell JW, *et al* (2015) Reversible centriole depletion with an inhibitor of Polo-like kinase 4. *Science*: 1–9

Woodruff JB (2021) The material state of centrosomes: lattice, liquid, or gel? *Curr Opin Struct Biol* 66: 139–147

Woodruff JB, Ferreira Gomes B, Widlund PO, Mahamid J, Honigmann A & Hyman AA (2017) The Centrosome Is a Selective Condensate that Nucleates Microtubules by Concentrating Tubulin. *Cell* 169: 1066-1077.e10

Woodruff JB, Wueseke O, Viscardi V, Mahamid J, Ochoa SD, Bunkenborg J, Widlund PO, Pozniakovsky A, Zanin E, Bahmanyar S, *et al* (2015a) Regulated assembly of a supramolecular centrosome scaffold in vitro. *Science* 348: 808–812

Woodruff JB, Wueseke O, Viscardi V, Mahamid J, Ochoa SD, Bunkenborg J, Widlund PO, Pozniakovsky A, Zanin E, Bahmanyar S, *et al* (2015b) Regulated assembly of a supramolecular centrosome scaffold in vitro. *Science* 348: 808–812

Wu H, Carvalho P & Voeltz GK (2018) Here, there, and everywhere: The importance of ER membrane contact sites. *Science* 361

Wueseke O, Zwicker D, Schwager A, Wong YL, Oegema K, Jülicher F, Hyman AA & Woodruff JB (2016) Polo-like kinase phosphorylation determines Caenorhabditis elegans centrosome size and density by biasing SPD-5 toward an assembly-competent conformation. *Biology Open* 5: 1431–1440

Xu J, Shen C, Wang T & Quan J (2013) Structural basis for the inhibition of Polo-like kinase 1. *Nat Struct Mol Biol* 20: 1047–1053

Zhu F, Lawo S, Bird A, Pinchev D, Ralph A, Richter C, Müller-Reichert T, Kittler R, Hyman AA & Pelletier L (2008) The mammalian SPD-2 ortholog Cep192 regulates centrosome biogenesis. 18: 136–141

Zwicker D, Decker M, Jaensch S, Hyman AA & Julicher F (2014) Centrosomes are autocatalytic droplets of pericentriolar material organized by centrioles. *Proceedings of the National Academy of Sciences* 111: E2636–E2645

Figure 1

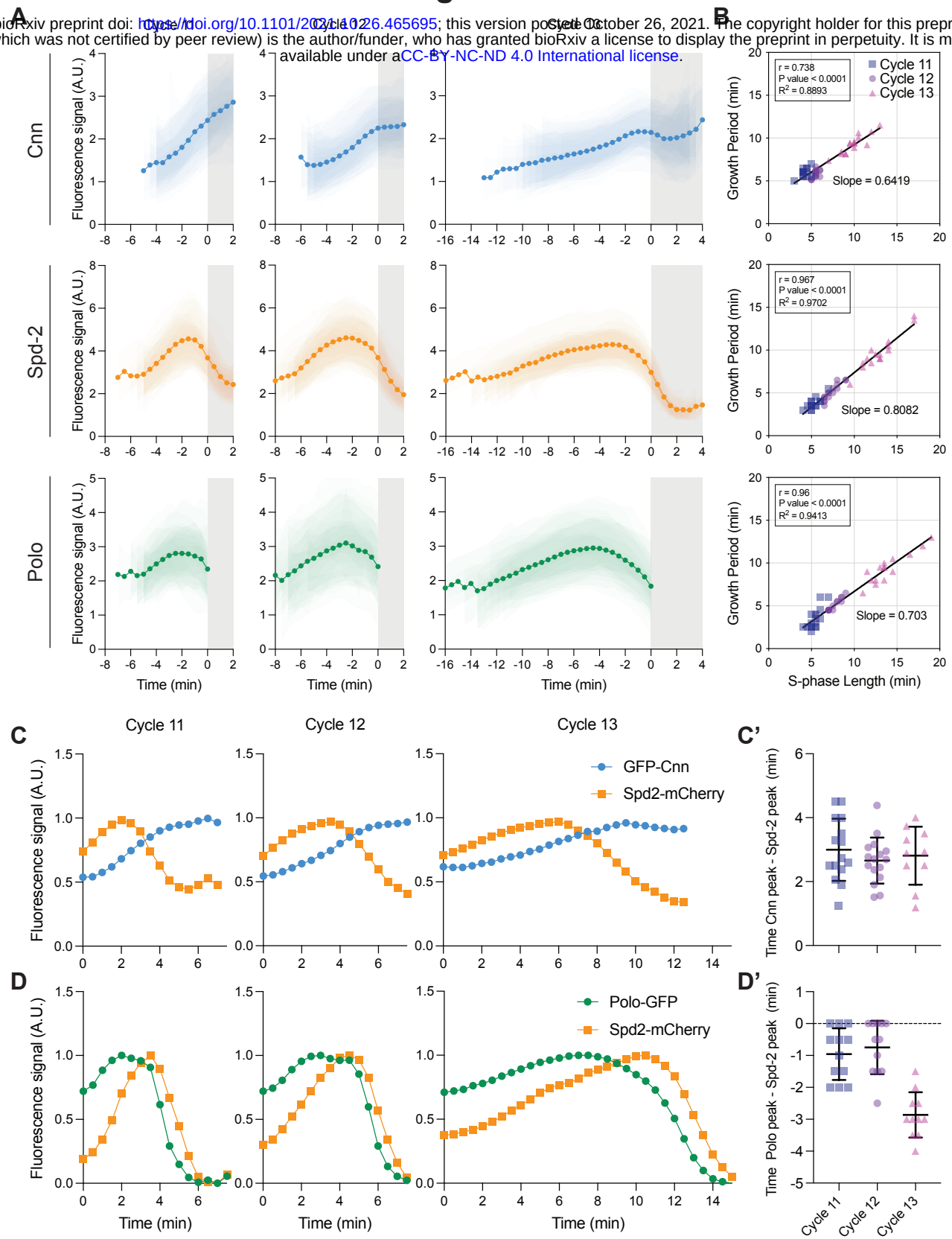

Analysis of PCM scaffold assembly dynamics during nuclear cycles 11-13

(A) Graphs show the average centrosomal fluorescence intensity of NG-Cnn, Spd-2-GFP, and Polo-GFP—*dark lines* (±SD for each individual embryo indicated in reduced opacity; N≥15 embryos)—over time during nuclear cycles 11, 12, and 13. The white parts of the graphs indicate S-phase and the grey parts mitosis. All individual embryo tracks were aligned to the start of mitosis (NEB; t=0). **(B)** Scatter plots show the correlation between the centrosome growth period and S-phase length for the embryos analysed in (A). Lines indicate mathematically regressed fits. The goodness of fit (R^2) was assessed in GraphPad Prism. The bivariate Gaussian distribution of the data was confirmed by Henze-Zirkler test, and the strength of correlation (*r*) and the statistical significance (*P-value*) were calculated using Pearson correlation test. **(C, D)** Graphs show the average centrosomal fluorescent intensity over time during nuclear cycles 11, 12 and 13 for embryos (N≥8) co-expressing Spd-2-mCherry (orange) with either GFP-Cnn (blue) (C) or Polo-GFP (green) (D). Fluorescence intensity was rescaled to between 0 and 1 in each cycle. **(C',D')** Dot plots compare the time difference between the peak Spd-2-mCherry levels and the peak GFP-Cnn (C') or peak Polo-GFP (D') levels in each embryo. Data are presented as Mean±SD.

Figure 2

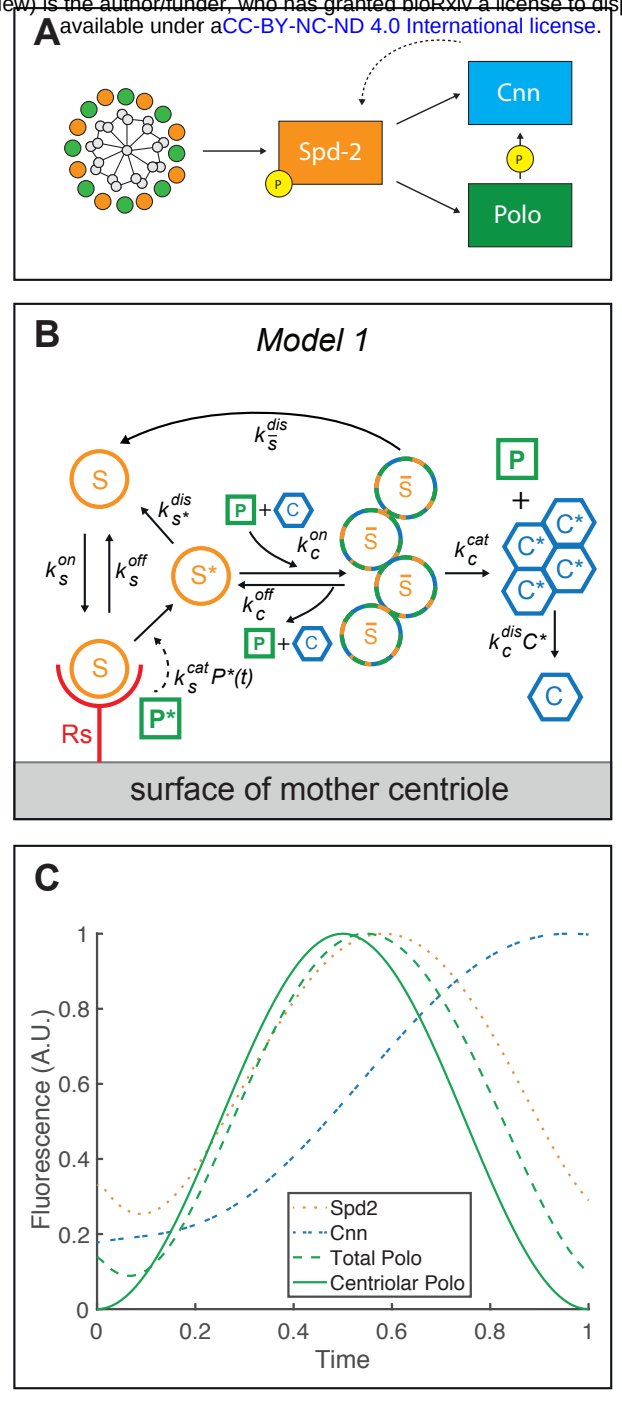

Mathematical modelling of PCM scaffold assembly

(A) A schematic summary of the putative molecular interactions that drive the assembly of a Spd-2/Polo/Cnn mitotic PCM scaffold in *Drosophila* (see main text for details). **(B)** Schematic illustrates a version of the molecular model of PCM scaffold assembly that can be formulated as a series of ODEs (see Materials and Methods), allowing us to calculate how the levels of each component in the system changes over time. **(C)** Graph shows the output from the model depicted in (B), illustrating how the centrosomal levels of the various PCM scaffold components change over time if a centriolar pulse of Polo activity (*solid green line*) is imposed on the system. Total Polo (*dotted green line*) represents the sum of the P^* generated at the centriole surface and the P^* bound to the $\bar{S}$ scaffold; Total Spd-2 (*dotted orange line*) represents the sum of Spd-2 in S^* and $\bar{S}$; Total Cnn (*dotted blue line*) represents the sum of Cnn in $\bar{S}$ and C^*. To better reflect the situation in vivo—where the centrosomes start each cycle already associated with some PCM scaffold acquired from the previous cycle (Conduit et al, 2010)—we allow the model to run for a complete initial cycle (where the levels of all scaffolding components start at zero) and then graph the behaviour of the system starting from this point during a second cycle. Thus, the pulse of centriolar Polo activity starts from zero at the start of the cycle, but some Polo, Spd-2 and Cnn recruited in the previous cycle are already present at the centrosome.

Figure 3

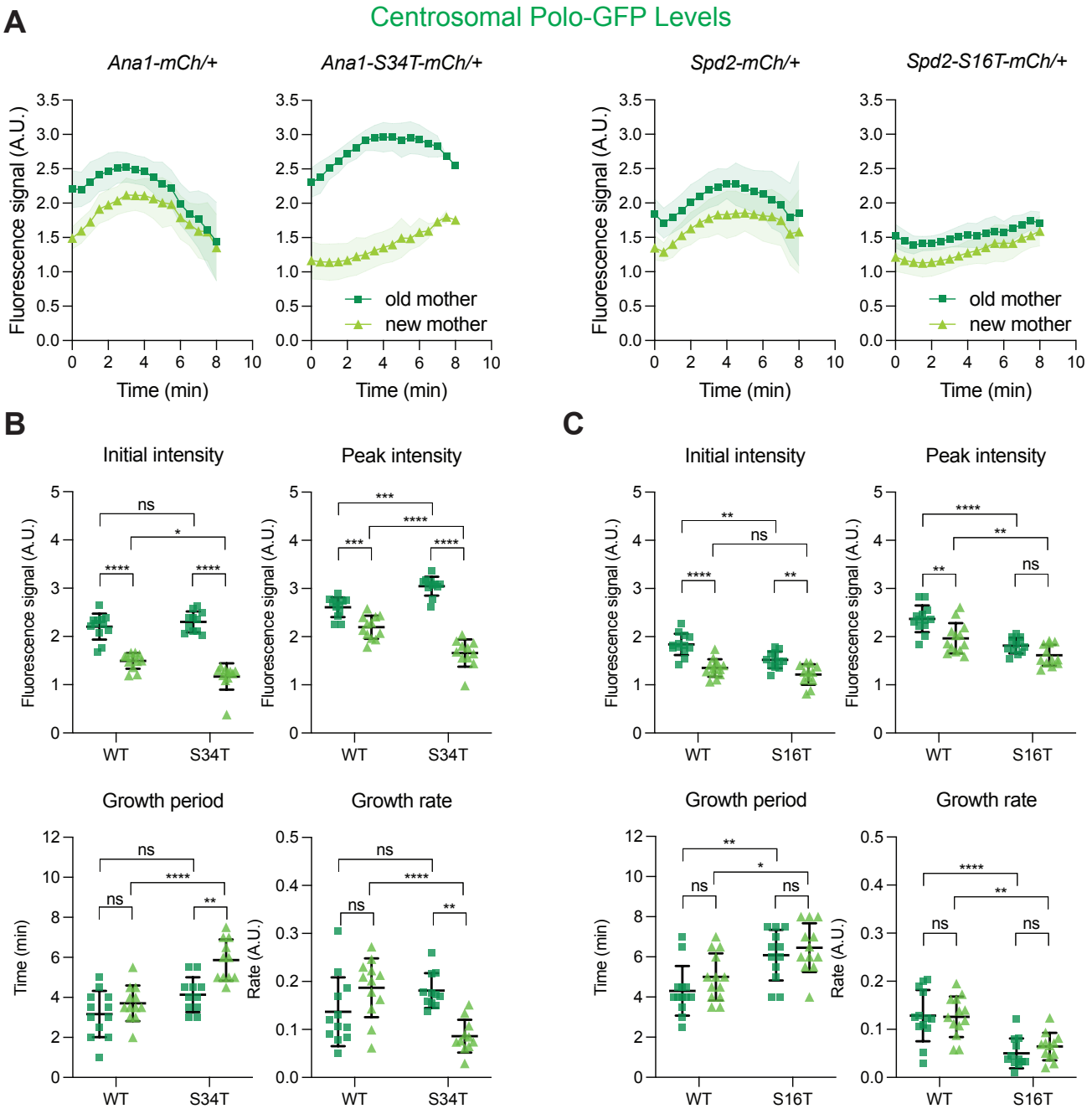

<u>Perturbing the ability of Ana1 or Spd-2 to recruit Polo perturbs the pulse of Polo activity</u>

(A) Graphs show how the average fluorescent intensity (±SD) of Polo-GFP changes over time at OM (*dark green squares*) or NM (*light green triangles*) centrosomes during nuclear cycle 12 in embryos (N=12) laid by WT females expressing either Ana1-mCherry, Ana1-S34T-mCherry, Spd-2-mCherry, or Spd-2-S16T-mCherry. In this experiment, embryos were aligned to the start of S-phase (t=0), which was scored by centriole separation. **(B, C)** Bar charts compare various growth parameters (indicated above each graph) of the embryos analysed in (A); dots representing the behaviour of OM and NM centrosomes in each class of embryo are shown in *dark green squares and light green triangles*, respectively. Statistical significance was first assessed by an ordinary two-way ANOVA, and then a Šídák's multiple comparisons test (*: P<0.05, **: P<0.01, ***: P<0.001, ****: P<0.0001, ns: not significant).

Figure 4

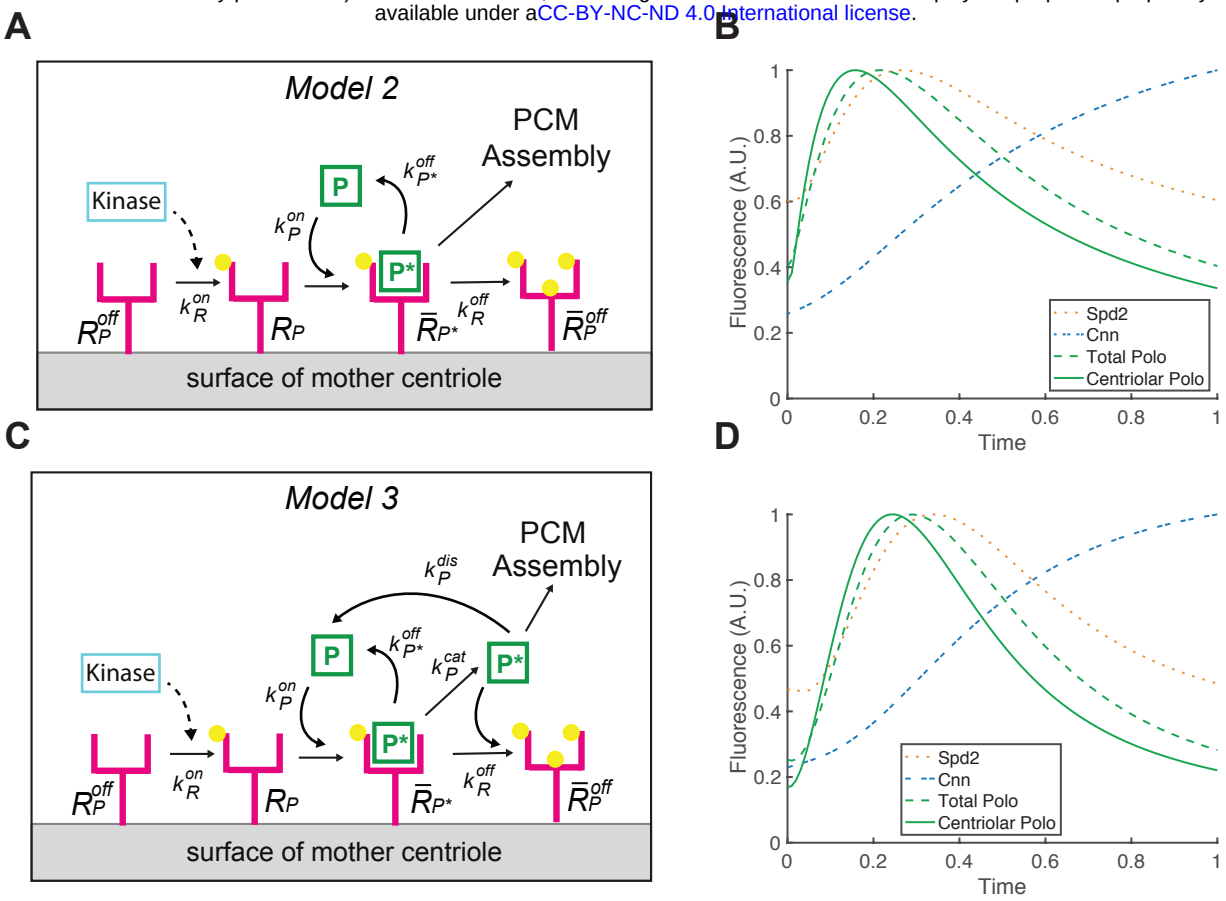

Mathematical modelling can explain how centrioles might generate a pulse of Polo activity

(A) Schematic illustrates a molecular model (*Model 2*) of how an interaction between Polo and its centriolar receptor can generate a pulse of centriolar Polo activity (see main text for details). **(B)** This model was formulated as a series of ODEs (see Materials and Methods) to allow us to graph how the levels of centriolar Polo would change over time (*solid green line*). The graph also illustrates the output when this pulse of Polo activity is fed into our earlier model of PCM scaffold assembly (Model 1, Figure 2A)—illustrating how the levels of total centrosomal Polo (*dotted green line*), Spd-2 (*dotted orange line*) and Cnn (*dotted blue line*) (as defined in the legend to Figure 2) change over time. As in Figure 2B, we allow the model to run for a complete initial cycle and then graph the behaviour of the system during a second cycle. **(C,D)** Same as (A), except the schematic (C) illustrates and the graph shows the output from (D) a slightly different molecular model (*Model 3*). In this model we allow the activated Polo generated by binding to its Receptors to remain active for a short period after it has been released from its Receptors.

Figure 5

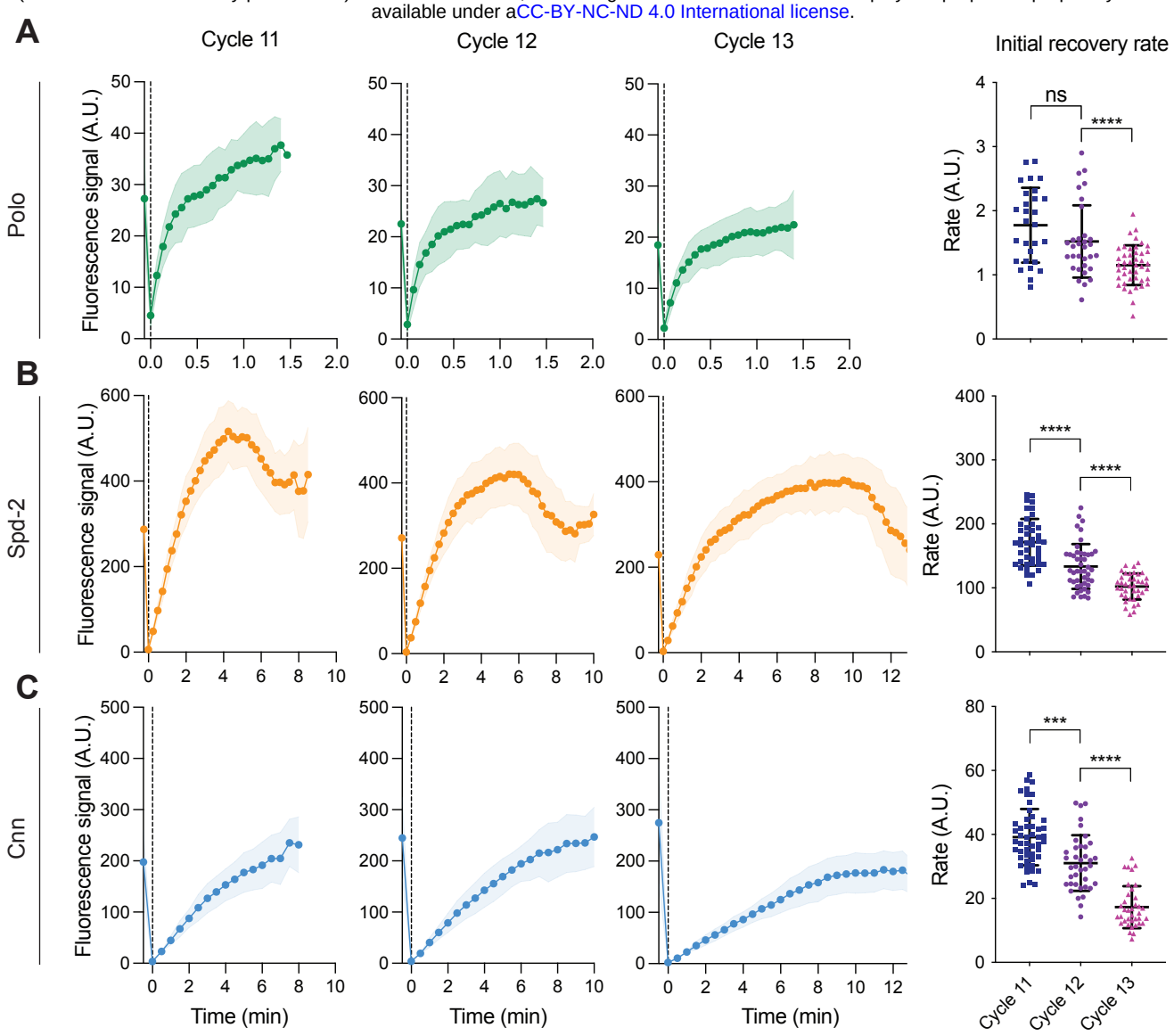

The rate of recruitment of Polo, Spd-2 and Cnn slows at successive nuclear cycles

Graphs show the recovery of centrosomal fluorescence intensity (±SD) after photobleaching of Polo-GFP (A; imaged every 4secs), Spd-NG (B; imaged every 15secs) and NG-Cnn (C; imaged every 30secs) in early S-phase of cycle 11, 12 or 13. Each coloured line is an average of a total of 25-50 centrosomes imaged from 10-12 embryos in each cycle. Dot plots compare the average initial recovery rate (±SD) of these proteins in nuclear cycle 11, 12, or 13. Statistical significance was assessed using a Dunnett's T3 multiple comparison test (ns: not significant, ***: P<0.001, ****: P<0.0001) after performing a Welch ANOVA test.

Figure 6

Centrosomal Polo Levels

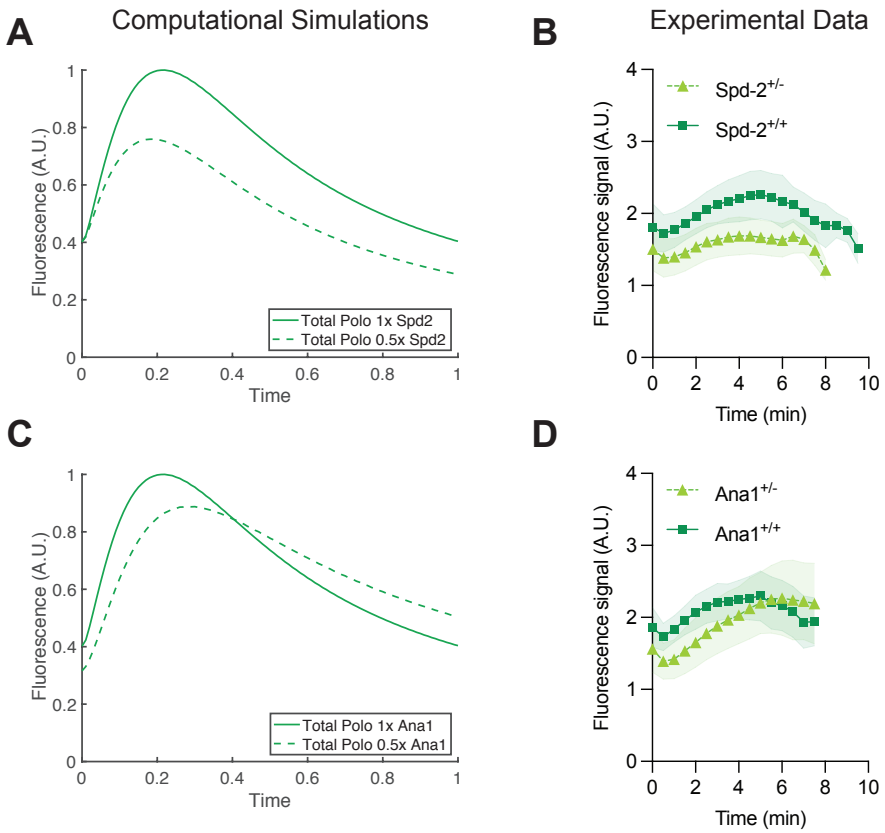

Mathematical models can predict the broad behaviour of the Polo pulse when the genetic dosage of *Spd-2* or *ana1* is halved

(**A,B**) Graphs compare computational simulations of the Polo pulse (generated using Model 3) in embryos expressing normal levels of Spd-2 (A) and Ana1 (B) (*solid green lines*) or in embryos where the levels of Spd-2 (A) or Ana1 (B) in the system have been halved (*dotted green lines*). (**C,D**) Graphs show *in vivo* data showing how the average centrosomal fluorescent intensity (±SD) of Polo-GFP changes over time during nuclear cycle 12 in embryos (N≥12) laid by either WT (+/+) females (*dark green squares*), or females in which the genetic dosage of *Spd-2* (A) or *ana1* (B) has been halved (+/-) (*light green triangles*).

Wong et al., Supplementary Material

Materials and Methods

Drosophila melanogaster stocks and husbandry

The *Drosophila* stocks used, generated and/or tested in this study are listed in Table 1; the precise stocks used in each experiment (and the relevant Figure) are listed in Table 2. Stocks were maintained on *Drosophila* culture medium (0.8% agar, 8% cornmeal, 1.8% yeast extract, 1% soya, 8% malt extract, 2.2% molasses, 0.14% nipagen, and 0.625% propionic acid) in 8cm x 2.5cm plastic vials or 0.25-pint plastic bottles.

Table 1*: Drosophila* stocks used in this study

Allele	Source
cnn^{f04547}	Exelixis stock no. f04547, Exelixis Stock Centre (Harvard Medical School, Boston, MA).
cnn^{HK21}	(Megraw *et al*, 1999; Vaizel-Ohayon & Schejter, 1999)
Ubq-NG-Cnn	Generated by Lisa Gartenmann; appears to be fully functional and rescues $cnn^{-/-}$ mutant.
Ubq-Spd-2-GFP	(Dix & Raff, 2007)
Spd-2-NG (CRISPR)	Generated for this study; appears to be fully functional and is homozygous viable and fertile.
$Spd\text{-}2^{z35711}$	(Giansanti *et al*, 2008)
$Spd\text{-}2^{G20143}$	(Dix & Raff, 2007)
Polo-TRAP-GFP	(Buszczak *et al*, 2007); appears to not be fully functional and is only viable as a heterozygote.
Ubq-Spd-2-mCherry	(Alvarez-Rodrigo *et al*, 2019)

ana1^{mecB}	(Blachon *et al*, 2009; Avidor-Reiss *et al*, 2004)
Ubq-Ana1-mCherry	(Alvarez-Rodrigo *et al*, 2020)
Ubq-Ana1-S34T-mCherry	(Alvarez-Rodrigo *et al*, 2020)
Ubq-Spd-2-S16T-mCherry	(Alvarez-Rodrigo *et al*, 2019); described in this previous publication as Spd-2-CONS.

Table 2: *Drosophila* stocks used in specific experiments

Genotype	Experiments	Figure
Ubq-NG-Cnn, cnn^{f04547} / cnn^{HK21}	1) Dynamics of NG-Cnn or Polo-GFP across nuclear cycles 11 – 13 2) Recovery rate of NG-Cnn or Polo-GFP in early S-phase of nuclear cycles 11 – 13 by FRAP	1A, 1B, 5C, S3
Polo-TRAP-GFP / +		1A, 1B, 5A, S3, 6A, 6B
Ubq-Spd-2-GFP ; Spd-2^{z35711} / Spd-2^{G20143}	Dynamics of Spd-2-GFP across nuclear cycle 11 – 13	1A, 1B
Spd-2-NG (CRISPR)	Recovery rate of Spd-2-NG in the early S-phase of nuclear cycles 11 – 13 by FRAP	5B, S3
cnn^{f04547}, Ubq-GFP-Cnn / cnn^{HK21} ; Ubq-Spd-2-mCherry, Spd-2^{G20143} / Spd-2^{z35711}	GFP-Cnn or Polo-GFP co-expressed with Spd-2-mCherry to measure the relative timing of their dynamics	1C
Polo-TRAP-GFP / Ubq-Spd-2-mCherry		1D

Ubq-Ana1-mCherry / + ; Polo-TRAP-GFP / +	Polo-GFP in the presence of Ana1-mCherry or Spd2-mCherry mutants that have significantly reduced number of Polo binding sites.	3A, 3B
Ubq-Ana1-S34T-mCherry / + ; Polo-TRAP-GFP / +		
Polo-TRAP-GFP / Ubq-Spd-2-mCherry, $spd2^{G20143}$		3A, 3C
Polo-TRAP-GFP / Ubq-Spd-2-S16T-mCherry, $spd2^{G20143}$		
Polo-TRAP-GFP / $Spd\text{-}2^{z35711}$	Polo-GFP with a reduced dosage of endogenous Spd-2 or Ana1	6A
Polo-TRAP-GFP / $ana1^{mecB}$		6B
cnn^{f04547} / cnn^{HK21}	Embryo without endogenous Cnn	S1
Ubq-NG-Cnn, cnn^{f04547} / +	NG-Cnn or GFP-Cnn used in this study with endogenous Cnn to compare their relative level	
cnn^{f04547}, Ubq-GFP-Cnn / +		
$Spd\text{-}2^{G20143}$ / $Spd\text{-}2^{z35711}$	Embryo without endogenous Spd-2	S1
Ubq-Spd-2-GFP ; $Spd\text{-}2^{z35711}$ / +	Spd-2-GFP or Spd-2-NG used in this study with endogenous Spd-2 to compare their relative level	
Spd-2-NG (CRISPR) / +		

Generation of CRISPR/Cas9-mediated fly line

A single guide RNA (sgRNA) and donor plasmid for homology-directed repair (HDR) were generated respectively, injected into Cas9-expressing CFD2 embryos and screened as previously described (Port *et al*, 2014). Briefly, the sgRNA target sequence was selected that was close to the insertion site using a sgRNA design algorithm as described

previously (Gratz *et al*, 2014), and cloned in pCFD3 plasmid as described previously (Port *et al*, 2014). The donor plasmid containing tandem DNA sequence of 1 kb upstream homology arm, linker plus mNeonGreen sequence and 1 kb downstream homology arm was synthesized by GENEWIZ Co. Ltd. (Suzhou, China) in pUC57. To enhance the recombination process and to linearize the plasmid in vivo, the cleavage sites (sgRNA target sequence) were introduced on either side of the 3kb sequence in the donor plasmid. In addition, the sgRNA target sequences within the homology arm of the donor plasmid were mutated (without affecting the amino acid sequence) to prevent the Cas9 from cleaving within the repair template and the knock-in construct once it had been inserted into the endogenous locus in vivo. The mixture of both the constructs -Guide RNA (sgRNA) and donor plasmid was injected into Cas9-expressing CFD2 embryos (Port *et al*, 2015) by the Department of Genetics, University of Cambridge (UK). After hatching, the single flies were crossed to a balancer line (PrDr/TM6C) and screened for the positive insertion event by PCR for 2 or 3 generations. The final generation of flies was balanced, and the gene sequence containing the 3kb insertion fragment and the region flanking the insertion was sequenced before conducting the experiments.

Embryo collections

Embryos were collected from plates (25% apple & raspberry juice, 2.5% sucrose, and 2.25% agar) supplemented with fresh yeast suspension. For imaging experiments, embryos were collected for 1h at 25^{o}C, and aged at 25^{o}C for 45–60 min. Embryos were dechorionated by hand, mounted on a strip of glue on a 35-mm glass-bottom Petri dish

with 14 mm micro-well (MatTek), and desiccated for 1 min at 25°C before covering with Voltalef grade H10S oil (Arkema).

Immunoblotting

Immunoblotting analysis to estimate protein expression level was performed as previously described (Aydogan et al., 2018). The following primary antibodies were used: rabbit anti-Spd-2 (1:500), rabbit anti-Cnn (1:1000), and rabbit anti-GAGA factor (1:500). HRP-conjugated donkey anti-rabbit (NA934V lot:17876631, Cytiva Lifescience) secondary antibodies were used at 1:3000.

Spinning disk confocal microscopy

Images of embryos were acquired at 23°C using a PerkinElmer ERS spinning disk confocal system mounted on a Zeiss Axiovet 200M microscope using Volocity software (PerkinElmer). A 63X, 1.4NA oil objective was used for all acquisition. The oil objective was covered with an immersion oil (ImmersolT 518 F, Carl Zeiss) with a refractive index of 1.518 to minimize spherical aberration. The detector used was a charge-coupled device (CCD) camera (Orca ER, Hamamatsu Photonics, 15-bit), with a gain of 200 V. The system was equipped with 405nm, 488nm, 561nm, and 642 solid-state lasers (Oxxius S.A.). All red/green fluorescently tagged samples were acquired using UltraVIEW ERS 'Emission Discrimination' setting. The emission filter of these images was set as followed: a green long-pass 520nm emission filter and a red long-pass 620nm emission filter. For dual channel imaging, the red channel was imaged before the green channel in every slice in a z-stacks. For Fluorescent Recovery after Photobleaching (FRAP) experiments,

circular regions of interests (ROI) of diameter 4 μm were defined around selected centrosomes of interest (multiple centrosomes were often selected from a single individual embryo). A 488 nm laser at 50% laser power was used to FRAP each sample in 10 iterations over a period of 2secs. 0.5-μm z-sections were acquired, with the number of sections, time step, laser power, and exposure depending on the experiment.

Data analysis

Raw time-series from imaged embryos were imported into Fiji. The photobleaching of raw time-series images was corrected using the exponential decay algorithm and images were z-projected using the maximum intensity projection function. The background was estimated and corrected by a uneven illumination background correction (Soille, 2004). The centrosomes were tracked using TrackMate (Tinevez *et al*, 2016). A custom Python script was then used to appropriately threshold and extract the fluorescence intensities of all of the tracked centrosomes as they changed over time in each individual embryo. To extract the features of the Spd-2 and Polo oscillations we measured the *initial intensity* of the centrosomes as they first separated in early S-phase and their *maximum intensity* at the oscillation peak; the time between these points represented the *growth period*, while the *growth rate* was calculated as: (*maximum intensity – initial intensity*)/*growth period*. To extract these features for Cnn, several mathematical models were fit to the data from each embryo, and the model that best fit the majority of the embryos was then applied to all embryos: *linear increase* (Cycle 11); *linear increase* + *plateau* (Cycle 12); *linear increase* + *linear decrease* (Cycle 13) (Table 3). The average *initial intensity*, *maximum*

intensity, *growth period* and *growth rate* were then calculated from the fitted data for each embryo.

For FRAP analysis, a tight bounding box was manually drawn around each centrosome (see tutorial in the Github repository of this publication), and the box was linked across multiple frames using a custom Python script. In experiments where the centrosomes organized by the old mother centriole and new mother centriole (OM and NM centrosomes, respectively) were tracked independently, two centrosomes with the shortest inter-centrosomal distance at the start of S-phase and within a preset distance threshold were annotated as a pair. The brighter centrosome in a pair was annotated as the OM while the dimmer one was annotated as NM (Conduit *et al*, 2010; Novak *et al*, 2014). The link to these custom Python scripts can be found on Github under the folder "Data analysis" (https://github.com/SiuShingWong/Wong-et-al-2021).

Table 3: Models used for feature extraction of the Cnn data

Centrosomal fluorescence of Cnn (Cycle 11)—Linear Increase
Equation: $Y = m * X + c$ *Initial intensity: c* *Maximum intensity:* $m * X_{last\_frame} - c$ *Growth Period:* X_{last_frame} *Growth Rate: m*
Centrosomal fluorescence of Cnn (Cycle 12)—Linear Increase + Plateau
Equation: $Y = m * X + c$ *when* $X < X_0$

Y = b when X > X_0 *where X_0 > 0, b > 0* *Initial Intensity: c* *Maximum Intensity: b* *Growth Period: X_0* *Growth Rate: m*
Centrosomal fluorescence of Cnn (Cycle 13)—Linear Increase + Linear Decrease
Equation: *Y = m_0 * X + c when X < X_0* *Y = m_1 * X + c when X > X_0* *where X_0 > 0, m_0 > 0, m_1 < 0* *Initial Intensity: c* *Maximum Intensity: m_0*X_0 + c* *Growth Period: X_0* *Growth Rate: m_0* *Decrease Rate: m_1*

Mathematical model of PCM scaffold assembly kinetics *(Model 1)*

We assume that centriolar Spd-2 receptors, R_S, are able to convert cytoplasmic Spd-2, S, into an unstable Spd-2 scaffold, S^*, via the complex $\bar{R}_S$. The on, off, and catalytic conversion rates of this process are k_S^{on}, k_S^{off}, and $k_S^{\text{cat}}P^*/n$, respectively, where $P^*(t)$ is the total amount of active Polo at time t and $n(t)$ is the number of centrioles in the embryo at time t (which will double after every cycle), so that P^*/n describes the amount of active Polo at each centriole. In the first instance, we do not attempt to model $P^*(t)$ but instead treat it as a given function which we use as an external stimulus for the system. Although

S^* is unstable, it can recruit cytoplasmic Cnn, C, and cytoplasmic Polo, P, to form the more stable complex $\bar{S}$, which can phosphorylate C to convert it into a stable Cnn scaffold form C^*. The on, off, and catalytic conversion rates of this process are k_C^{on}, k_C^{off}, and k_C^{cat}, respectively. The two scaffold forms of Spd-2 have disassembly rates $k_{S^*}^{\text{dis}}$ and $k_{\bar{S}}^{\text{dis}}$, respectively, while the disassembly rate of the Cnn scaffold is given by $k_C^{\text{dis}} C^*/n$, as we assume that this disassembly rate is proportional to the size of the Cnn scaffold surrounding each centriole since the Cnn scaffold largely disassembles from its outer surface (Conduit et al., 2010).

The previous description can be summarised as a system of reactions

$$R_S + S \underset{k_S^{\text{off}}}{\overset{k_S^{\text{on}}}{\leftrightarrow}} \bar{R}_S \xrightarrow{\frac{k_S^{\text{cat}} P^*}{n}} R_S + S^*, \tag{1}$$

$$S^* + C + P \underset{k_C^{\text{off}}}{\overset{k_C^{\text{on}}}{\leftrightarrow}} \bar{S} \xrightarrow{k_C^{\text{cat}}} S^* + C^* + P, \tag{2}$$

$$S^* \xrightarrow{k_{S^*}^{\text{dis}}} S, \tag{3}$$

$$\bar{S} \xrightarrow{k_{\bar{S}}^{\text{dis}}} S + C + P, \tag{4}$$

$$C^* \xrightarrow{\frac{k_C^{\text{dis}} C^*}{n}} C. \tag{5}$$

For simplicity, we assume that cytoplasmic species diffuse sufficiently fast in the embryo that we may treat these variables as spatially homogeneous, and therefore we neglect spatial effects from the model. By imposing the law of mass action, we derive the following system of four ordinary differential equations (note that the explicit dependence in the dependent variables on time has been dropped)

$$\frac{d\bar{R}_S}{dt} = k_S^{\text{on}} R_S S - \left(k_S^{\text{off}} + \frac{k_S^{\text{cat}} P^*}{n} \right) \bar{R}_S, \tag{6}$$

$$\frac{dS^*}{dt} = \frac{k_S^{\text{cat}} P^* \bar{R}_S}{n} - k_C^{\text{on}} C P S^* + (k_C^{\text{off}} + k_C^{\text{cat}}) \bar{S} - k_{S^*}^{\text{dis}} S^*, \tag{7}$$

$$\frac{d\bar{S}}{dt} = k_C^{\text{on}} C P S^* - (k_C^{\text{off}} + k_C^{\text{cat}}) \bar{S} - k_{\bar{S}}^{\text{dis}} \bar{S}, \tag{8}$$

$$\frac{dC^*}{dt} = k_C^{\text{cat}} \bar{S} - \frac{k_C^{\text{dis}} C^{*2}}{n}, \tag{9}$$

where the PCM quantities, $S^*, \bar{S}, C^*, P^*, R_S$ and $\bar{R}_S$ are defined as the total number of the corresponding species in the embryo (i.e. dimensionless units), and the cytoplasmic quantities, $S, C,$ and P, are defined as the volumetric concentration of the corresponding species (i.e. units m^{-3}). We assume, for simplicity, that the embryo is a closed system which implies that the total amount Spd-2 (S_0) and Cnn (C_0) in the embryo is conserved. Further, since the total amount of Polo (P_0) is large we treat cytoplasmic Polo as a prescribed constant unaffected by absorption into the scaffold. Finally, we assume that the total number of Spd-2 receptors in the embryo is proportional to the number of centrioles. These constraints read

$$R_S + \bar{R}_S = r_{S_0} n, \tag{10}$$

$$\bar{R}_S + VS + S^* + \bar{S} = S_0, \tag{11}$$

$$VC + C^* + \bar{S} = C_0, \tag{12}$$

$$VP = P_0, \tag{13}$$

where r_{S_0} is the total number of receptors per centriole and V is the volume of the embryo.

These equations describe the total amount of each species in the embryo. However, it is useful to describe the model on a per-centriole basis. We do this by defining the auxiliary

(lower case) per-centriole variables: $R_S = nr_S$, $\bar{R}_S = n\bar{r}_S$, $S^* = ns^*$, $\bar{S} = n\bar{s}$, $C^* = nc^*$, and $P^* = np^*$. In terms of these variables, our system reads

$$\frac{d\bar{r}_S}{dt} = k_S^{\text{on}} r_S S - \left(k_S^{\text{off}} + k_S^{\text{cat}} p^*\right)\bar{r}_S - \frac{\bar{r}_S}{n}\frac{dn}{dt}, \tag{14}$$

$$\frac{ds^*}{dt} = k_S^{\text{cat}} p^* \bar{r}_S - \frac{k_C^{\text{on}} C P_0 s^*}{V} + \left(k_C^{\text{off}} + k_C^{\text{cat}}\right)\bar{s} - k_{S^*}^{\text{dis}} s^* - \frac{s^*}{n}\frac{dn}{dt}, \tag{15}$$

$$\frac{d\bar{s}}{dt} = \frac{k_C^{\text{on}} C P_0 s^*}{V} - \left(k_C^{\text{off}} + k_C^{\text{cat}}\right)\bar{s} - k_{\bar{S}}^{\text{dis}} \bar{s} - \frac{\bar{s}}{n}\frac{dn}{dt}, \tag{16}$$

$$\frac{dc^*}{dt} = k_C^{\text{cat}} \bar{s} - k_C^{\text{dis}} c^{*2} - \frac{c^*}{n}\frac{dn}{dt}, \tag{17}$$

subject to

$$r_S + \bar{r}_S = r_{S_0}, \tag{18}$$

$$VS + n(\bar{r}_S + s^* + \bar{s}) = S_0, \tag{19}$$

$$VC + n(c^* + \bar{s}) = C_0. \tag{20}$$

While equations (14) – (20), subject to the appropriate initial conditions, are sufficient to describe the system, it is convenient for its mathematical analysis to instead formulate the model in terms of "dimensionless" variables. Through this process, we determine the dimensionless parameter groups (e.g. the ratio of the reaction rates to the cell cycle timescale) which govern the dynamics of the system, which in turn enables us to simplify the system and reduce the number of independent variables in the model. We non-dimensionalise the system by using the following scalings

$$r_S, \bar{r}_S, s^*, \bar{s}, c^* \sim r_{S_0}, \qquad S \sim \frac{S_0}{V}, \qquad C \sim \frac{C_0}{V}, \qquad p^* \sim p_{\max}, \qquad t \sim T, \tag{21}$$

where T is the typical period of the cell cycle, and $p_{\max}$ is the maximum amplitude of the imposed Polo activity. In terms of dimensionless variables, the model reads

$$\frac{d\bar{r}_S}{dt} = K_S^{\text{on}} r_S S - \left(K_S^{\text{off}} + K_S^{\text{cat}} p^*\right)\bar{r}_S - \frac{\bar{r}_S}{n}\frac{dn}{dt}, \tag{22}$$

$$\frac{ds^*}{dt} = K_S^{\text{cat}} p^* \bar{r}_S - K_C^{\text{on}} C s^* + (K_C^{\text{off}} + K_C^{\text{cat}})\bar{s} - K_{S^*}^{\text{dis}} s^* - \frac{s^*}{n}\frac{dn}{dt}, \tag{23}$$

$$\frac{d\bar{s}}{dt} = K_C^{\text{on}} C s^* - (K_C^{\text{off}} + K_C^{\text{cat}})\bar{s} - K_{\bar{S}}^{\text{dis}} \bar{s} - \frac{\bar{s}}{n}\frac{dn}{dt}, \tag{24}$$

$$\frac{dc^*}{dt} = K_C^{\text{cat}} \bar{s} - K_C^{\text{dis}} c^{*2} - \frac{c^*}{n}\frac{dn}{dt}, \tag{25}$$

subject to

$$r_S + \bar{r}_S = 1, \tag{26}$$

$$S + \delta_S n(\bar{r}_S + s^* + \bar{s}) = 1, \tag{27}$$

$$C + \delta_C n(c^* + \bar{s}) = 1, \tag{28}$$

where

$$K_S^{\text{on}} = k_S^{\text{on}} T S_0/V, \quad K_S^{\text{off}} = k_S^{\text{off}} T, \quad K_S^{\text{cat}} = k_S^{\text{cat}} p_{\text{max}} T, \quad K_{S^*}^{\text{dis}} = k_{S^*}^{\text{dis}} T, \quad K_{\bar{S}}^{\text{dis}} = k_{\bar{S}}^{\text{dis}} T,$$

$$K_C^{\text{on}} = k_C^{\text{on}} T C_0 P_0/V^2, \quad K_C^{\text{off}} = k_C^{\text{off}} T, \quad K_C^{\text{cat}} = k_C^{\text{on}} T, \quad K_C^{\text{dis}} = k_C^{\text{dis}} r_{S_0} T,$$

$$\delta_S = \frac{r_{S_0}}{S_0}, \quad \delta_C = \frac{r_{S_0}}{C_0}, \quad \delta_{p^*} = \frac{r_{S_0}}{p_{\text{max}}}. \tag{29}$$

Given a solution to this system, the total size of the Spd-2 and Cnn scaffolds and total amount of active Polo surrounding each centriole are given by

$$S_{\text{tot}} = \bar{r}_S + s^* + \bar{s}, \tag{30}$$

$$C_{\text{tot}} = c^* + \bar{s}, \tag{31}$$

$$P_{\text{tot}} = p^* + \delta_{p^*}\bar{s}, \tag{32}$$

where S_{tot}, C_{tot}, and P_{tot} are dimensionally scaled with S_0, C_0, and p_{max}, respectively.

To allow us to compare accurately the output from our models to the experimental data we first determined reasonable initial conditions, as the centrosomes in our experiments are already initially associated with some PCM (that was acquired in the previous cycle)

at the start of S-phase. To do this, we first solve (22) – (28) subject to the initial conditions $\bar{r}_S = s^* = \bar{s} = c^* = 0$. (i.e. no Spd-2 or Cnn scaffold is assembled around the centriole). Since the system is approximately cyclic, we then use the final values output by this solution, $\bar{r}_S = \bar{r}_{S_0}$, $s^* = s_0^*$, $\bar{s} = \bar{s}_0$, as our new initial values. Since the Cnn scaffold divides and partially breaks away during centriole separation, we cannot impose the cyclic condition on Cnn. However, since the output value for c^* is of order 1 in the rescaled variables, we set $c^* = 1$ as our new initial value for the Cnn scaffold. In this way, the centrioles in our model start the cycle already associated with some Spd-2 and Cnn scaffold that they acquired in the previous cycle, as is the case with our experimental data.

In Figure 2B, we plot the incorporation of Spd-2 and Cnn into the PCM, S_{tot} and C_{tot}, over the duration of a single cycle by solving (22) – (28) subject to the initial conditions $\bar{r}_S = \bar{r}_{S_0}$, $s^* = s_0^*$, $\bar{s} = \bar{s}_0$, $c^* = 1$, the parameter values given in **Table 4**, and the constraint that the number of centrioles is constant during the cycle, $n \equiv 1$ without loss of generality. We also plot the prescribed Polo activity (i.e. the oscillation in $p^*(t)$ that we impose on the system), $p^*(t) := \frac{1}{2}(1 - \cos(2\pi t))$, and the total Polo at the centriole, P_{tot}. The amplitudes in all the solutions have been normalised to 1.

Table 4: Initial Conditions and Parameters used in Model 1

K_S^{on}	20	K_S^{off}	200	K_S^{cat}	100
K_C^{on}	100	K_C^{off}	100	K_C^{cat}	50
$K_{S^*}^{\text{dis}}$	20	$K_{\bar{S}}^{\text{dis}}$	1	K_C^{dis}	0.05

δ_S	0.001	δ_C	0.001	δ_{p^*}	10

Mathematical model of centriolar Polo activity *(Model 2)*

Model 1 assumed a given oscillation in Polo. Next, we describe a model for how such an oscillation in Polo activity might be generated by the centriole through the interaction between Polo and its receptors at the centriole surface, such as Ana1 (Alvarez-Rodrigo et al., 2021). We assume that these receptors, R_P^{off}, are initially inactive and unable to bind Polo. To initiate mitotic PCM assembly, the receptors are activated at a rate k_R^{on} due to their phosphorylation by a protein kinase, which is most likely a Cdk/Cyclin, or a kinase that is regulated by the Cdk/Cyclins (such as Polo or Aurora A). This new form, which we denote R_P, is able to bind Polo with on and off rates k_P^{on} and k_P^{off}, respectively, to form the complex $\bar{R}_P$. We assume that the Polo in this complex is active and able to initiate mitotic PCM assembly as described by Model 1. We also assume that this active form of Polo instigates the deactivation of the receptors at a rate $k_R^{\text{off}}P^*/n$. This final form, which we denote $\bar{R}_P^{\text{off}}$, is unable to bind or activate Polo. This system likely resets itself between cycles when $\bar{R}_P^{\text{off}}$ is dephosphorylated to regenerate R_P^{off}, but we do not model this reset here. Finally, we assume that the reactions occurring in the PCM are the same as before, with the active centriolar Polo (in this instance given by $P^* \equiv \bar{R}_P$) now forming part of the solution to our model. The reactions describing the generation of Polo read

$$R_P^{\text{off}} \xrightarrow{k_R^{\text{on}}} R_P, \tag{33}$$

$$R_P + P \underset{k_P^{\text{off}}}{\overset{k_P^{\text{on}}}{\leftrightarrow}} \bar{R}_P, \tag{34}$$

$$R_P \xrightarrow{\frac{k_R^{\text{off}}P^*}{n}} \bar{R}_P^{\text{off}}, \tag{35}$$

By imposing the law of mass action, we obtain the following system of ODEs,

$$\frac{dR_P^{\text{off}}}{dt} = -k_R^{\text{on}} R_P^{\text{off}}, \tag{36}$$

$$\frac{dR_P}{dt} = k_R^{\text{on}} R_P^{\text{off}} - k_P^{\text{on}} P R_P + k_P^{\text{off}} \bar{R}_P - \frac{k_R^{\text{off}} P^*}{n} R_P, \tag{37}$$

$$\frac{d\bar{R}_P}{dt} = k_P^{\text{on}} P R_P - k_P^{\text{off}} \bar{R}_P, \tag{38}$$

$$\frac{d\bar{R}_P^{\text{off}}}{dt} = \frac{k_R^{\text{off}} P^*}{n} R_P, \tag{39}$$

$$P^* = \bar{R}_P, \tag{40}$$

We also assume that the total number of Polo receptors at each centriole, r_{P_0}, is conserved, which reads

$$R_P^{\text{off}} + R_P + \bar{R}_P + \bar{R}_P^{\text{off}} = n r_{P_0}. \tag{41}$$

As before, we write the system in per-centriole variables, and non-dimensionalise by setting $R_P^{\text{off}} = n r_{P_0} r_P^{\text{off}}$, $R_P = n r_{P_0} r_P$, $\bar{R}_P = n \bar{R}_P r_{P_0}$, and $\bar{R}_P^{\text{off}} = n r_{P_0} \bar{r}_P^{\text{off}}$, and $P^* = n r_{P_0} p^*$ so that the dimensionless model reads

$$\frac{dr_P^{\text{off}}}{dt} = -K_R^{\text{on}} r_P^{\text{off}}, \tag{42}$$

$$\frac{dr_P}{dt} = K_R^{\text{on}} r_P^{\text{off}} - K_P^{\text{on}} r_P + K_P^{\text{off}} \bar{r}_P - K_R^{\text{off}} p^* r_P, \tag{43}$$

$$\frac{d\bar{r}_P}{dt} = K_P^{\text{on}} r_P - K_P^{\text{off}} \bar{r}_P, \tag{44}$$

$$\frac{d\bar{r}_P^{\text{off}}}{dt} = K_R^{\text{off}} p^* r_P, \tag{45}$$

$$p^* = \bar{r}_P, \tag{46}$$

subject to

$$r_P^{\text{off}} + r_P + \bar{r}_P + \bar{r}_P^{\text{off}} = 1, \tag{47}$$

where

$$K_P^{\text{on}} = k_P^{\text{on}} P_0 T, \qquad K_P^{\text{off}} = k_P^{\text{off}} T, \qquad K_R^{\text{on}} = k_R^{\text{on}} T, \qquad K_R^{\text{off}} = k_R^{\text{off}} r_{P_0} T. \tag{48}$$

Note that we have scaled P^* with r_{P_0} in this instance rather than $p_{\max}$ since the maximum amplitude of the Polo activity is not known *a priori.,* and, since the receptors generate the active Polo in this model, this is the correct scaling for P^*.

In this model, the total amount of Polo in the centrosome is given by

$$P_{\text{tot}} = p^* + \delta_r \bar{s}, \tag{49}$$

where $\delta_r = \frac{r_{S_0}}{r_{P_0}}$.

As before, to determine the appropriate initial conditions, we first solve the model subject to $r_P = \bar{r}_P = \bar{r}_S = s^* = \bar{s} = c^* = 0, r_P^{\text{off}} = 1$ to compute the output $r_{P_0}, \bar{r}_{P_0}, \bar{r}_{S_0}, s_0^*, \bar{s}_0, c_0^*$. Our new initial conditions are then given by setting $r_P = r_{P_0}$, $\bar{r}_P = \bar{r}_{P_0}$, $\bar{r}_S = \bar{r}_{S_0}$, $s^* = s_0^*$, $\bar{s} = \bar{s}_0$, $r_P^{\text{off}} = 1 - r_{P_0} - \bar{r}_{P_0}$.

In Figure 4A, we plot the centriolar Polo, p^*, the total Polo, P_{tot}, the Spd2 scaffold size, S_{tot}, and the Cnn scaffold size C_{tot}, found by solving (22) – (28) and (43) – (48) with the parameter values given in **Tables 4 and 5**. As before, to determine the appropriate initial conditions, we first solve the model subject to $r_P = \bar{r}_P = \bar{r}_S = s^* = \bar{s} = c^* = 0, r_P^{\text{off}} = 1$ to compute the output $r_{P_0}, \bar{r}_{P_0}, \bar{r}_{S_0}, s_0^*, \bar{s}_0$. Our new initial conditions are then given by setting $r_P = r_{P_0}$, $\bar{r}_P = \bar{r}_{P_0}$, $\bar{r}_S = \bar{r}_{S_0}$, $s^* = s_0^*$, $\bar{s} = \bar{s}_0$, $r_P^{\text{off}} = 1 - r_{P_0} - \bar{r}_{P_0}$, and $c^* = 1$. All solutions have been normalised.

In Figure 6, we plot the total Polo under normal conditions (parameter values given in Tables 1 and 2) as well as half dose Ana1 ($r_{P_0} \to 0.5 r_{P_0}$, i.e. $\delta_r \to 2\delta_r$ and $K_R^{\text{off}} \to 0.5 K_R^{\text{off}}$) and half dose Spd2 ($S_0 \to 0.5 S_0$, i.e. $\delta_S \to 2\delta_S$ and $K_S^{\text{on}} \to 0.5 K_S^{\text{on}}$). All solutions have been normalised with respect to the wild type solution.

Table 5: Initial Conditions and Parameters used in Model 2 and Model 3

K_P^{on}	100	K_P^{off}	50	K_P^{cat}	20	K_P^{dis}	10
K_R^{on}	10	K_R^{off}	20	δ_r	5		

Mathematical model of centriolar Polo activity *(Model 3)*

We also considered a variation on the model for centriolar Polo activity in which, in addition to the reactions described in Model 2, the Polo-receptor complex, $\bar{R}_P$, is also able to release active Polo into the cytoplasm at a rate k_P^{cat}. In this model, the receptors effectively catalyse the activation of Polo, which has the ability to diffuse and phosphorylate local substrates before it becomes inactivated. We believe that this might better reflect the in vivo situation because Polo turns-over rapidly at centrioles and centrosomes ($t_{1/2}$ ~ 10secs; Figure 5). We allow this active cytoplasmic Polo, P_c^*, to deactivate/dissolve at a rate k_P^{dis}. In this model, the total active centriolar Polo is given by $P^* = P_c^* + \bar{R}_P$. The full system of reactions in this model reads

$$R_P^{\text{off}} \to^{k_R^{\text{on}}} R_P, \tag{50}$$

$$R_P + P \underset{k_P^{\text{off}}}{\overset{k_P^{\text{on}}}{\leftrightarrow}} \bar{R}_P \to^{k_P^{\text{cat}}} R_P + P_c^*, \tag{51}$$

$$R_P \to^{\frac{k_R^{\text{off}} P^*}{n}} \bar{R}_P^{\text{off}}, \tag{52}$$

$$P_c^* \rightarrow^{k_P^{\text{dis}}} P. \tag{53}$$

Following the same methodology as before, and nondimensionalising the active cytoplasmic Polo according to $P_c^* = nr_{P_0}p_c^*$, yields

$$\frac{dr_P^{\text{off}}}{dt} = -K_R^{\text{on}} r_P^{\text{off}}, \tag{54}$$

$$\frac{dr_P}{dt} = K_R^{\text{on}} r_P^{\text{off}} - K_P^{\text{on}} r_P + \left(K_P^{\text{off}} + K_P^{\text{cat}}\right)\bar{r}_P - K_R^{\text{off}} p^* r_P, \tag{55}$$

$$\frac{d\bar{r}_P}{dt} = K_P^{\text{on}} r_P - \left(K_P^{\text{off}} + K_P^{\text{cat}}\right)\bar{r}_P, \tag{56}$$

$$\frac{d\bar{r}_P^{\text{off}}}{dt} = K_R^{\text{off}} p^* r_P, \tag{57}$$

$$\frac{dp_c^*}{dt} = K_P^{\text{cat}} \bar{r}_P - K_P^{\text{dis}} p_c^*. \tag{58}$$

$$p^* = p_c^* + \bar{r}_P, \tag{59}$$

subject to

$$r_P^{\text{off}} + r_P + \bar{r}_P + \bar{r}_P^{\text{off}} = 1, \tag{60}$$

where

$$K_P^{\text{cat}} = k_P^{\text{cat}} T, \qquad K_P^{\text{dis}} = k_P^{\text{dis}} T, \tag{61}$$

and all other variables are defined as before.

In Figure 4B, we plot the generated centriolar Polo, p^*, the total Polo, P_{tot}, the Spd2 scaffold size, S_{tot}, and the Cnn scaffold size C_{tot}, found by solving (22) – (28) and (54) – (60) with parameter values given in **Tables 4 and 5**. The initial conditions are determined in the same manner as Model 2. All solutions have been normalised.

The MATLAB scripts to recapitulate the findings of all models can be found on Github under the folder "Mathematical modelling" (https://github.com/SiuShingWong/Wong-et-al-2021).

Statistical analysis

The details of statistical tests, sample size, and definition of the centre and dispersion are provided in individual Figure legends.

References for Materials and Methods

Alvarez-Rodrigo I, Steinacker TL, Saurya S, Conduit PT, Baumbach J, Novak ZA, Aydogan MG, Wainman A & Raff JW (2019) Evidence that a positive feedback loop drives centrosome maturation in fly embryos. *eLife* 8

Alvarez-Rodrigo I, Wainman A & Raff JW (2020) Ana1 recruits PLK1 to mother centrioles to promote mitotic PCM assembly and centriole elongation. *bioRxiv*: 2020.08.11.244194 doi:10.1101/2020.08.11.244194 [PREPRINT]

Avidor-Reiss T, Maer AM, Koundakjian E, Polyanovsky A, Keil T, Subramaniam S & Zuker CS (2004) Decoding cilia function: Defining specialized genes required for compartmentalized cilia biogenesis. *Cell* 117: 527–539

Blachon S, Cai X, Roberts KA, Yang K, Polyanovsky A, Church A & Avidor-Reiss T (2009) A proximal centriole-like structure is present in drosophila spermatids and can serve as a model to study centriole duplication. *Genetics* 182: 133–144

Buszczak M, Paterno S, Lighthouse D, Bachman J, Planck J, Owen S, Skora AD, Nystul TG, Ohlstein B, Allen A, *et al* (2007) The carnegie protein trap library: A versatile tool for drosophila developmental studies. *Genetics* 175: 1505–1531

Conduit PT, Brunk K, Dobbelaere J, Dix CI, Lucas EP & Raff JW (2010) Centrioles regulate centrosome size by controlling the rate of Cnn incorporation into the PCM. *Curr Biol* 20: 2178–2186

Dix CI & Raff JW (2007) Drosophila Spd-2 recruits PCM to the sperm centriole, but Is dispensable for centriole duplication. *Current Biology* 17: 1759–1764

Giansanti MG, Bucciarelli E, Bonaccorsi S & Gatti M (2008) Drosophila SPD-2 is an essential centriole component required for PCM recruitment and astral-microtubule nucleation. *Current Biology* 18: 303–309

Gratz SJ, Ukken FP, Rubinstein CD, Thiede G, Donohue LK, Cummings AM & O'Connor-Giles KM (2014) Highly specific and efficient CRISPR/Cas9-catalyzed homology-directed repair in Drosophila. *Genetics* 196: 961–971

Megraw TL, Li K, Kao LR & Kaufman TC (1999) The centrosomin protein is required for centrosome assembly and function during cleavage in Drosophila. *Development* 126: 2829–2839

Novak ZA, Conduit PT, Wainman A & Raff JW (2014) Asterless licenses daughter centrioles to duplicate for the first time in Drosophila embryos. *Curr Biol* 24: 1276–1282

Port F, Chen H-M, Lee T & Bullock SL (2014) Optimized CRISPR/Cas tools for efficient germline and somatic genome engineering in Drosophila. *Proc Natl Acad Sci USA* 111: E2967-76

Port F, Muschalik N & Bullock SL (2015) Systematic Evaluation of Drosophila CRISPR Tools Reveals Safe and Robust Alternatives to Autonomous Gene Drives in Basic Research. *G3 (Bethesda)* 5: 1493–1502

Soille P (2004) Background Notions. In *Morphological Image Analysis: Principles and Applications*, Soille P (ed) pp 15–62. Berlin, Heidelberg: Springer

Tinevez J-Y, Perry N, Schindelin J, Hoopes GM, Reynolds GD, Laplantine E, Bednarek SY, Shorte SL & Eliceiri KW (2016) TrackMate: An open and extensible platform for single-particle tracking. *Methods* 115: 80–90

Vaizel-Ohayon D & Schejter ED (1999) Mutations in centrosomin reveal requirements for centrosomal function during early Drosophila embryogenesis. *Current Biology* 9: 889–898

Figure S1

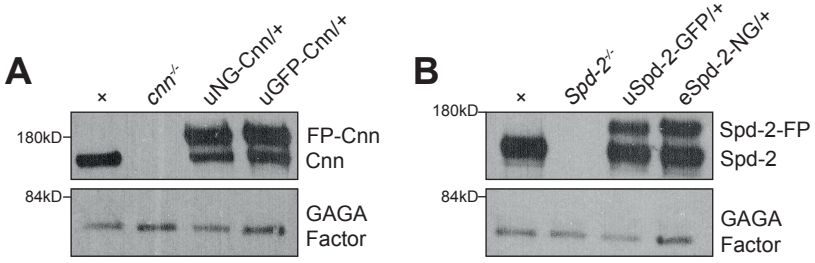

Analysing the relative expression levels of the fluorescent fusion-proteins used to quantify centrosome recruitment dynamics

(A,B) Western blots compare the relative expression levels in syncytial embryos of the GFP- and NG-fusion proteins (FP) used here to quantify the centrosomal recruitment dynamics of Cnn (A) or Spd-2 (B). This analysis reveals that GFP-Cnn and NG-Cnn expressed transgenically from the ubiquitin promoter (u) are present at slightly higher levels than the endogenous untagged Cnn. In contrast, Spd-2-GFP expressed transgenically from the ubiquitin promoter (u) and Spd-2-NG expressed as a CRISPR knock-in at the endogenous Spd-2 locus (e) are both present at slightly lower levels than the endogenous protein. Western blots of serial-dilutions of these samples indicate that the uNG-Cnn and uGFP-Cnn are overexpressed by ~2-3 fold compared to the endogenous protein, and that uSpd-2-GFP and eSpd-2-NG are underexpressed by ~2 fold. These blots were also probed with anti-GAGA factor antibodies as a loading control (Raff *et al*, 1994).

Figure S2

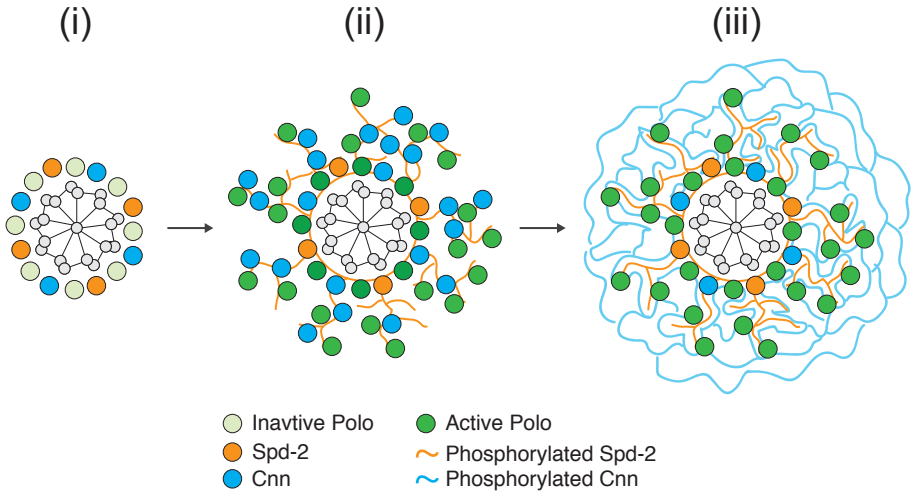

A molecular model of how Spd-2, Polo and Cnn cooperate to form a mitotic PCM scaffold

Cartoon illustrates the assembly of the Spd-2/Polo/Cnn mitotic PCM scaffold in *Drosophila*. During interphase **(i)**, Spd-2, Polo and Cnn are recruited to a toroid that surrounds the mother centriole (Fu & Glover, 2012). Polo is presumably inactive, and Spd-2 and Cnn are presumably not phosphorylated. As cells prepare to enter mitosis **(ii)**, Polo is activated at the centriole and the centrosomal Spd-2 becomes phosphorylated, allowing it to assemble into a scaffold that can flux outwards away from the centriole. The phosphorylated Spd-2 scaffold (equivalent to S^* in Figure 2B) is structurally weak, but it can recruit Polo—via phosphorylated S-S(P)/T(P) motifs (Alvarez-Rodrigo et al, 2019)—and also Cnn (Conduit et al, 2014b) to form the more stable $\bar{S}$ scaffold depicted in Figure 2B. The Polo recruited by Spd-2 is activated and can phosphorylate Cnn, allowing Cnn to assemble into a strong macromolecular scaffold (C^* in Figure 2B) that can flux outwards away from the Spd-2 scaffold (Conduit et al, 2014a; Feng et al, 2017). Cnn itself cannot recruit more Spd-2 or Polo, but it stabilises the expanding Spd-2 scaffold, so allowing Spd-2 to accumulate around the mother centriole **(iii)** (Conduit et al, 2014b).

Figure S3

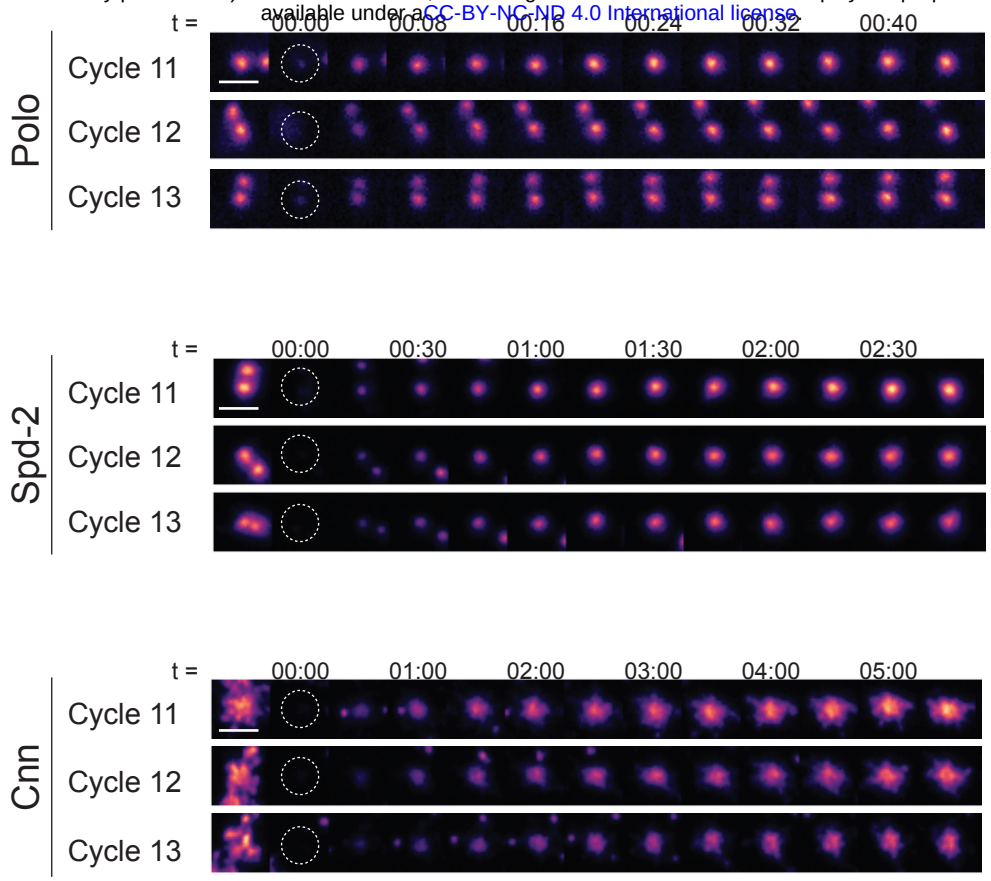

Monitoring rates of centrosomal fluorescence recovery of photobleached PCM scaffold components

Micrographs show examples of centrosomes that were fluorescently-labelled with either Polo-GFP, Spd-2-NG or NG-Cnn, photobleached at t=0, and then monitored for the subsequent recovery of fluorescence at the start of either nuclear cycle 11, 12 or 13. Time (mins:secs) is indicated above selected images (note the different time scales used for each fusion protein). Scale bar = 2μm.